



**HAL**  
open science

# Automatic geomorphological mapping using ground truth data with coverage sampling and random forest algorithms

Paul Aimé Latsouck Faye, Elodie Brunel, Thomas Claverie, Solym Mawaki Manou-Abi, Sophie Dabo-Niang

## ► To cite this version:

Paul Aimé Latsouck Faye, Elodie Brunel, Thomas Claverie, Solym Mawaki Manou-Abi, Sophie Dabo-Niang. Automatic geomorphological mapping using ground truth data with coverage sampling and random forest algorithms. Earth Science Informatics, In press, 10.1007/s12145-024-01347-x . hal-04624799

**HAL Id: hal-04624799**

**<https://hal.science/hal-04624799v1>**

Submitted on 25 Jun 2024

**HAL** is a multi-disciplinary open access archive for the deposit and dissemination of scientific research documents, whether they are published or not. The documents may come from teaching and research institutions in France or abroad, or from public or private research centers.

L'archive ouverte pluridisciplinaire **HAL**, est destinée au dépôt et à la diffusion de documents scientifiques de niveau recherche, publiés ou non, émanant des établissements d'enseignement et de recherche français ou étrangers, des laboratoires publics ou privés.

1 Automatic geomorphological mapping using  
2 ground truth data with coverage sampling and  
3 random forest algorithms

4 Faye Paul Aimé Latsouck<sup>1\*</sup>, Brunel Elodie<sup>1†</sup>, Claverie Thomas<sup>2†</sup>,  
5 Manou-Abi Solym<sup>1,3,5†</sup>, Dabo-Niang Sophie<sup>4†</sup>

6 <sup>1</sup> IMAG, University of Montpellier, CNRS, 34090, Montpellier, France .

7 <sup>2</sup> UMR ENTROPIE, IRD, IFREMER, CNRS, Univ La Réunion, Saint  
8 Denis, 97744, Réunion, France .

9 <sup>3</sup> CUFR, Centre Universitaire de Formation et de Recherche, Dombéni,  
10 97660, Mayotte, France .

11 <sup>4</sup> PAINLEVE UMR 8524, University of Lille, CNRS, INRIA-MODAL,  
12 59665, Lille, France .

13 <sup>5</sup> Laboratoire de Mathématiques et Applications UMR 7348 , University  
14 of Poitiers, CNRS, Futuroscope, 86073, Poitiers, France .

15 \*Corresponding author(s). E-mail(s):

16 [paul-aime-latsouck.faye@umontpellier.fr](mailto:paul-aime-latsouck.faye@umontpellier.fr);

17 Contributing authors: [elodie.brunel-piccinini@umontpellier.fr](mailto:elodie.brunel-piccinini@umontpellier.fr);

18 [tclaverie@gmail.com](mailto:tclaverie@gmail.com); [solym.manou-abi@univ-mayotte.fr](mailto:solym.manou-abi@univ-mayotte.fr);

19 [sophie.dabo@univ-lille.fr](mailto:sophie.dabo@univ-lille.fr);

20 †These authors contributed equally to this work.

21 **Abstract**

22 Marine geomorphological maps are useful to understand seafloor structure for  
23 example in the context of ecological studies, resources management or con-  
24 servation planning. Although techniques to build such maps are increasingly  
25 sophisticated, manual techniques are still largely used. Automated approaches  
26 are needed to get reproducible maps in a reasonable time. This work provides  
27 statistical learning approaches based framework to build automatically geomor-  
28 phological maps. We used bathymetric data to build Digital Bathymetric Model  
29 (DBM) and compute terrain attributes characteristic of seafloor geomorphol-  
30 ogy. Then, we used clustering based algorithms to select automatically ground

31 truth locations from a reference geomorphological map manually made. Finally  
32 a supervised classification model random forest based was used to build predic-  
33 tive models for seafloor geomorphology typologies. Subsequently we studied the  
34 effect of DBM resolution, sample size and sampling method of the ground truth  
35 locations, in the quality of map production via a series of simulations. Results  
36 showed that the proposed framework allowed to build efficiently relevant seafloor  
37 geomorphological maps. The best compromise between the sampling effort and  
38 the quality of the resulting maps was obtained with 100 m DBM resolution, 200  
39 data points sample size and using a complexity-dependent sampling method and  
40 led to a map matching at 90% the reference one.

41 **Keywords:** geomorphological map, spatial modeling, random forest classification,  
42 digital bathymetric model, terrain attributes, lidar data

43 **Declarations**

44 **Compliance with Ethical Standards**

45 All accepted principles of ethical and professional conduct have been followed during  
46 this research in accordance with Springer's standards.

47 **Funding**

48 No funding was received for conducting this study.

49 **Conflict of Interest**

50 On behalf of all authors, the corresponding author states that there is no conflict of  
51 interest.

52 **Ethical Approval**

53 This manuscript has not been published, accepted for publication, or under editorial  
54 review for publication elsewhere.

55 **Informed Consent**

56 The authors have given the informed consent to publish this article in the Journal of  
57 Geovisualization and Spatial Analysis if accepted.

58 **Code Availability**

59 The R code created during this work is open source and can be accessed in Zenodo  
60 repositories : <https://doi.org/10.5281/zenodo.8436795>

61 **Aknowledgments**

62 EPICURE program provides the bathymetric data used in this project. We are thank-  
63 ful to Rodolphe Devillers and Christophe Crambes for their field support. We thank  
64 Baptiste Chapuisat, Ghislain Durif and François David Collain for their assistance in  
65 High Performance Computing techniques. We also thank meso@LR for computational  
66 resources provided for the simulations carried out in this work.

# 67 1 Introduction

68 Geomorphological maps are georeferenced delineation of morphological structure and  
69 surface composition of a studied land and/or seafloor (Otto and Smith, 2013; Dramis  
70 et al, 2011; Pavlopoulos et al, 2009). Marine geomorphological maps are particularly  
71 crucial for resource management, conservation efforts, hazard assessment, protected  
72 area management, effective marine research campaign planning and various marine-  
73 related industrial works (Kienholz, 1978; Bishop et al, 2012; Fukunaga et al, 2019;  
74 Browne et al, 2010). Such maps provide valuable information on the composition and  
75 structure of the seabed which, among other usage, is needed to generate habitat maps  
76 through the identification and delineation of different benthic ecosystems like coral  
77 reefs, seagrass beds or various deep-sea communities (Pandian et al, 2009; Dramis  
78 et al, 2011; Wabnitz et al, 2008).

79 To produce geomorphological maps, different approaches are used (Siart et al, 2009;  
80 Hugenholtz et al, 2013). Widely used imagery techniques involve studying the pat-  
81 terns, textures, shapes, and color variations present in the imagery. This can be done  
82 manually by digitizing or tracing the features on the imagery or through automated  
83 or semi-automated image segmentation and classification techniques in Geographical  
84 Information System (GIS) using available image analysis tools. While imagery can be  
85 a valuable tool, it has a limited use for mapping deeply submerged geomorphological  
86 features due to water opacity. In such conditions, only acoustic approaches can pro-  
87 vide usable data which are generally completed by punctual carefully located ground  
88 truthing observations using for example scuba-divers or submarine-divers observation,  
89 Remote Operated Vehicle (ROV) or Automatic Underwater Vehicle (AUV) picture  
90 or videos, drop cameras or seabed sampling (Wynn et al, 2014; Locker et al, 2010).  
91 Subsequent treatments, required to generate maps with such data, will be to first pro-  
92 pose a geomorphologic category for each ground truthing point (ie. Typology), then  
93 delineate surfaces of homogeneous typologies. Depending on whether ground truthing  
94 points are defined as categories or as quantitative data, interpolation methodologies  
95 within the surface to be mapped might take different forms.

96 Many semi-automated or automated approaches have been also proposed in recent  
97 decades to achieve objective, automated and repeatable approach to extract mean-  
98 ingful information using vast quantities of data (Summers et al, 2021). Object-Based  
99 Image Analysis (OBIA) which use bathymetric derivatives or a combination of bathy-  
100 metric derivatives and backscatter to automatically segment the seafloor (Masetti et al,  
101 2018; Argyropoulou et al, 2016; Lacharité et al, 2018; Koop et al, 2021; Dekavalla  
102 and Argialas, 2017) are widely used. Bathymorphon / geomorphon-based classification  
103 (Jasiewicz and Stepinski, 2013; Sowers et al, 2020; Ahn et al, 2023; Novaczek et al,  
104 2019) and fuzzy logic scheme (Schmidt and Hewitt, 2004; Lucieer and Lucieer, 2009;  
105 Janowski et al, 2021) have been also investigated. The past 10 years, machine learning  
106 (Maschmeyer et al, 2019; Misiuk et al, 2021; Janowski et al, 2022; Sklar et al, 2024)  
107 and deep learning models (Behrens et al, 2018; Azarafza et al, 2023; Arhant et al,  
108 2023) has increasingly been used for geomorphological mapping. Furtherthmore, the  
109 performance of these statistical learning methods has also been investigated in com-  
110 parison with manually ones (Van der Meij et al, 2022; Diesing et al, 2014). In recent  
111 years, although these methods have proven their effectiveness, they are often combined

112 with underwater imagery which superseded expert manual interpretation and are par-  
113 ticularly costly for large scale mapping (Van der Meij et al, 2022; Cui et al, 2021;  
114 Galvez et al, 2022; Misiuk and Brown, 2023; Breyer et al, 2023). As alternative, this  
115 work provides a clustering based algorithm for an optimal ground truth sampling and  
116 a learning-based approach for automatic geomorphological mapping. It focuses on the  
117 classical situation where experts use morphological map to define surfaces and ground  
118 truth measure to define typologies. But to that respect, further considerations need to  
119 be addressed: (i) the quality of bathymetric data required, (ii) the typology definition,  
120 and (iii) the methodology to use for creating geomorphological maps with such data.  
121 (i) Bathymetry is recognized as essential when mapping geomorphology (Wilson et al,  
122 2007; Lecours et al, 2016; Fukunaga et al, 2019). It is particularly useful for identify-  
123 ing and delineating submerged landforms that are not visible in aerial images. Modern  
124 bathymetric systems can provide high-resolution data, capturing fine-scale details of  
125 the seafloor morphology. Their accuracy is often higher compared to aerial images, as  
126 it directly measures the water depth and seafloor elevation. However, the selection of  
127 the appropriate technology is crucial to ensure the acquisition of accurate and reliable  
128 data suited for an optimal geomorphological map production. More precisely equip-  
129 ment and material setup will depend on factors such as the scale and coverage needed,  
130 water depth, desired resolution, sampling effort and budgetary considerations. Com-  
131 promise between the sampling effort and the quality of the data have to be made but  
132 little tools are available to choose the most optimal setup. Indeed very high-resolution  
133 data may be necessary for detailed local studies, while coarser resolution data might  
134 suffice for larger-scale regional or global analyses. In the present research, some exam-  
135 ples to help on such decisions are proposed.

136 (ii) A typology is a description of one geomorphological category of seabed (in our  
137 case). However, to make a geomorphological map usable, comparable and understand-  
138 able by a large international community, categories definition of typologies need to  
139 form a consensus. Our study is based on the Millennium Coral Reef Mapping Project  
140 (MCRMP) typologies. Initiated by the Institute for Marine Remote Sensing - Univer-  
141 sity of South Florida (IMaRS/USF) in 2001 and continued since 2003 by reasearchers  
142 of the Institut de Recherche pour le Développement (IRD), the MCRMP has proposed  
143 a multi-level hierarchical structure (Andréfouët et al, 2004). MCRMP typologies were  
144 widely used as they enable several sites around the world to be compared on a the-  
145 matically rich, homogeneous basis (Andréfouët and Dirberg, 2006). These typologies  
146 provide a description of coral reef geomorphology distinguishing reef units such as  
147 slopes, flats, passes, terraces, lagoons, channels, etc.

148 (iii) Several approaches can be chosen to generate geomorphological maps from pre-  
149 viously described data. The most classical approach is to manually draw typologies  
150 envelopes using GIS softwares (Minár and Evans, 2008; Otto et al, 2018). However,  
151 it is tedious and poorly replicable if temporal changes need to be monitored. Auto-  
152 mated approaches are of several kind. This work focuses on statistical learning based  
153 approaches for their ability to efficiently process and analyze large volumes of spatial  
154 data, to learn complex relationships present in the data leading to improved accu-  
155 racy in produced maps (Stepinski et al, 2007; Siqueira et al, 2022; Van der Meij et al,  
156 2022). More precisely four steps are followed : 1) generate a Digital Bathymetric Model

157 (DBM) from bathymetric data, 2) compute terrain attributes from DBM on the entire  
158 surface studied, 3) train random forest based classification algorithm to match terrain  
159 attributes with ground truthing typologies and 4) predict typologies from the entire  
160 surface studied using the classification model generated.

161 The chosen methodology to generate geomorphological map was tested on a classi-  
162 cal tropical reef feature: an atoll mapping from South Western Indian Ocean. Our  
163 approach is to propose a sensitivity analysis based on a comparison with an existing  
164 expert map while degrading DBM definition as proxy of data acquisition setup and  
165 varying the number of ground truth points as well as the methodology to select their  
166 locations as proxy of field effort. The ultimate goal is to supply tools to plan mapping  
167 field campaign using coverage sampling algorithms, codes to semi-automate geomor-  
168 phological mapping procedure using random forest algorithm and propose metrics to  
169 evaluate the quality of the map generated across different resolutions. Recommenda-  
170 tions to choose the DBM resolution, ground truth size and sites selection are also  
171 provided.

## 172 2 Materials and methods

### 173 2.1 Data

174 For this work, bathymetric data (depth measurements) collected between 2009 and  
175 2010 on Geyser atoll with a surface area of approximately 268 km<sup>2</sup> are used  
176 (Figure 1A). A set of 48.10<sup>6</sup> data points were collected by LIDAR 1 m resolution cali-  
177 brated. The depth range captured by this tool often reaches down to -30 m but due to  
178 exceptional very good water clarity conditions, bathymetric records on Geyser range  
179 between -50 and 4 meters (see their distribution in Figure S1). This data is available  
180 on the Hydrography and Oceanography Service of the Navy website <sup>1</sup>.

181 An expert geomorphological map of the Geyser atoll available here <sup>2</sup> is also used. This  
182 scale-free map was produced by manual contouring, resulting from expert interpreta-  
183 tion of hyperspectral images. 11 geomorphological typologies have been identified on  
184 Geyser (Roos et al, 2017).

### 185 2.2 General methodology

186 Here an automated scheme using bathymetry and some field typologies verifications  
187 also called ground truth to generate reproducible geomorphological maps is used (see  
188 Figure S2 in the supplemental materials). The methodology is the following: 1) Using  
189 bathymetric data, a Digital Bathymetric Model (DBM) is created at a given resolu-  
190 tion. 2) From the DBM, terrain attributes corresponding to raster layers which have  
191 the potential to influence seafloor geomorphology are computed. 3) Using a given  
192 coordinate sampling method, a given number of ground truth locations is drawn.  
193 By overlaying these locations with the expert map, geomorphological typologies are  
194 attributed to each ground truth points. 4) Using the training set of coupled terrain  
195 attributes and ground truth typologies, a recursive feature elimination algorithm based

---

<sup>1</sup><https://data.shom.fr/donnees>

<sup>2</sup><https://sextant.ifremer.fr/geonetwork/srv/api/records/21232c12-e409-4136-a24a-78c346518cfa>

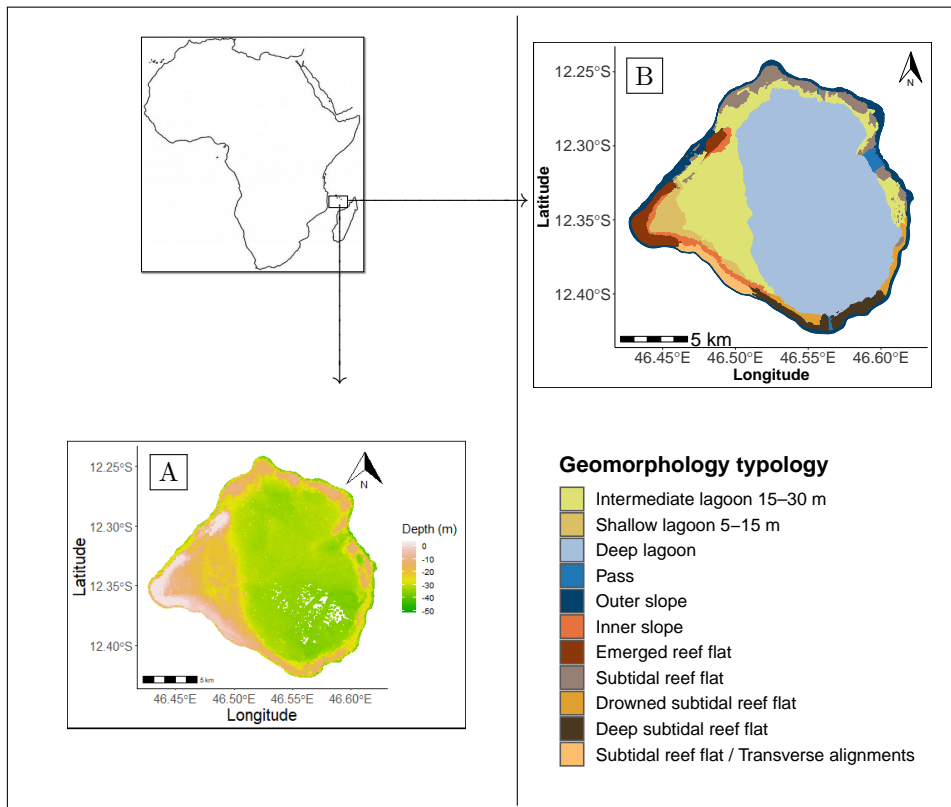


**Fig. 1** Geyser is an atoll in the Western Indian ocean, specifically located in the northern Mozambique channel between Mayotte and the Gloriosos Islands and covering approximately 268 km<sup>2</sup>. **A** Bathymetry data (in meters) collected by LIDAR technology and provided by Hydrography and Oceanography Service of the Navy (SHOM). **B** Geomorphologic structure identified for the Geyser atoll, as a part of the EPICURE project (Roos et al, 2017).

196 on a random forest classifier is used to select most relevant covariates. The latter are  
 197 then used to train a random forest based predictive model for geomorphologic typologies.  
 198 This model is finally used to predict geomorphologic typologies on the whole  
 199 study site. 5) The quality of the map production was then evaluated using two types  
 200 of performance criteria: the model performance (Balanced accuracy) and the match-  
 201 ing between the generated map and the expert map (Match and Balanced match).  
 202 The robustness of our approach is also evaluated using a sensitivity analysis through  
 203 simulation by varying bathymetric data definition, numbers of ground truth points and  
 204 methodology to select their locations. This involved in examining five DBM resolutions  
 205 (5 m, 25 m, 50 m, 100 m and 500 m), six sample sizes (50, 100, 200, 500, 700, 1000)  
 206 and three sampling methods (two spatial coverage sampling methods denoted SCS-  
 207 KMEANS and SCS-CLARA, and a complexity-dependent sampling method denoted  
 208 CDS). For each of these combinations ( $5 \times 6 \times 3$ ), 30 replicates of geomorphological  
 209 maps are generated by replicating the steps 3-5 described above.



### 2.2.1 Digital Bathymetric Model creation

The raw bathymetric dataset contains approximately  $48.10^6$  data points giving latitude, longitude and depth values. To avoid numerical issues due to redundant observations, this dataset was spatially sub-sampled and data points are kept as homogeneous as possible using the *buffer.points* function in the supplemental materials (Roberts, 2015). The sub-sampled data are such that each retained data point is at least at a distance of 5 m from one another. Following this procedure, the new dataset of approximately  $8.10^6$  data points obtained is used to generate the DBM which consists in the creation of a square grid of  $T^2$  cells or rasters. The cell size define the DBM resolution. Different resolutions (5 m, 25 m, 50 m, 100 m, 500 m)<sup>3</sup> are created using the *dbm* function proposed in the supplemental materials. The bathymetry or depth value of each cell is calculated by taking the average of all the depths inside the same cell.

Furthermore, some deep areas are poorly sampled, due to the lack of signal return on the LIDAR sensor (see white zone in the middle of Figure 1A). To get a depth measure for each ground truth location selected using one of the automatic sampling methodology presented further, depth measure on each raster of the study area were required. Thus for each DBM resolution, missing depth of empty cells in this zone are interpolated using an ordinary kriging model via the *ok.dbm* function provided in the supplemental materials. The kriging method is not described in details since the problem of missing data is out of the scope of the paper (Cressie, 1988). In contrast, empirical results provided in the supplemental materials show that it performs better than five others spatial interpolation methods for our data Table S1. This imputation method allows to complete bathymetric data on these cells.

### 2.2.2 Terrain attributes calculation

It consists in quantifying predictors for seafloor geomorphology. For each DBM resolution, terrain attributes were calculated using a moving routine from the DBM. More precisely, let us denote the depth  $D_{i,j}$  of a given cell with  $(i, j) \in \llbracket 1, T \rrbracket \times \llbracket 1, T \rrbracket$  and consider the depth  $D_{i+k, j+l}$  of the neighboring cells with  $(k, l) \in \mathcal{D}_3 = \llbracket -1, 1 \rrbracket \times \llbracket -1, 1 \rrbracket$ . These cells are defining the  $3 \times 3$  window on which the terrain attributes are defined. Note that it is possible to generalize the study to square window with size greater than 3. Selected terrain attributes can be organised into three groups: Slope (*Slope*) and orientation (*Aspect*) measures, terrain variability measures such as Roughness (*Roughness*), Terrain ruggedness index (*TRI*) and Vector ruggedness measure (*VRM*) and curvature and relative position measures such as Profile convexity (*profc*), Planform convexity (*planc*) and Bathymetric position index (*BPI*).

Slope has been widely recognized as an important factor for determining benthic habitat and colonization and has been used in many marine studies (Copeland et al, 2013; Fukunaga et al, 2019; Sterne et al, 2020). Like the magnitude of the steepest drop

---

<sup>3</sup>The 5 m resolution is the one used by biologists during field verification campaigns. We then looked for a very high resolution at which the geomorphological maps produced were degraded because they were too pixelated. 500 m seemed to be a good choice. Between these two resolutions, we empirically searched for intermediate resolutions enabling us to obtain "significantly" different maps. Hence the 25 m, 50 m and 100 m resolutions were retained.

249 in depth, *Slope* (in degrees) is derived from rates of change in  $x$  (longitude) and  $y$   
 250 (latitude) directions and is calculated as follows, for each cell  $(i, j) \in \llbracket 1, T \rrbracket \times \llbracket 1, T \rrbracket$ ,

$$Slope_{i,j} = \frac{180}{\pi} \arctan \left( \sqrt{\left(\frac{\partial D_{i,j}}{\partial x}\right)^2 + \left(\frac{\partial D_{i,j}}{\partial y}\right)^2} \right). \quad (1)$$

where

$$\begin{cases} \frac{\partial D_{i,j}}{\partial x} = [(D_{i+1,j+1} + 2D_{i+1,j} + D_{i+1,j-1}) - (D_{i-1,j+1} + 2D_{i-1,j} + D_{i-1,j-1})]/8\Delta. \\ \frac{\partial D_{i,j}}{\partial y} = [(D_{i+1,j+1} + 2D_{i,j+1} + D_{i-1,j+1}) - (D_{i+1,j-1} + 2D_{i,j-1} + D_{i-1,j-1})]/8\Delta. \end{cases}$$

251 where the real number  $\Delta$  stands for the cell size of the grid.

252 The orientation measure (*Aspect*) gives the exposure of a given area to such water  
 253 waves and is often used in the calculation of others parameters that directly influ-  
 254 ence habitat (Wilson et al, 2007). *Aspect* (in degrees) is the compass direction of the  
 255 steepest drop in depth and is calculated as follows, for each cell  $(i, j) \in \llbracket 1, T \rrbracket \times \llbracket 1, T \rrbracket$ ,

$$Aspect_{i,j} = 180 + \frac{180}{\pi} \arctan \left( \frac{\partial D_{i,j}}{\partial x} + \frac{\partial D_{i,j}}{\partial y} \right). \quad (2)$$

256 The roughness measure (*Roughness*) is a critical factor affecting ecological and phys-  
 257 ical processes on the reef (Leon et al, 2015; Dartnell, 2000). It corresponds to the  
 258 difference between the maximum and minimum depth values over a  $3 \times 3$  window and  
 259 is defined for each cell  $(i, j) \in \llbracket 1, T \rrbracket \times \llbracket 1, T \rrbracket$  as follows:

$$Roughness_{i,j} = \max_{k,l \in \mathcal{D}_3} (D_{i+k,j+l}) - \min_{k,l \in \mathcal{D}_3} (D_{i+k,j+l}). \quad (3)$$

260 The Terrain Ruggedness Index (*TRI*), is a terrestrial ruggedness measure (Riley et al,  
 261 1999) that was adapted to bathymetry data to highlight morphological heterogeneity  
 262 (Valentine et al, 2004; Rozycka et al, 2017). It is defined as the mean of the absolute  
 263 differences between the depth value of a cell and the one of its neighboring cells, for  
 264 each cell  $(i, j) \in \llbracket 1, T \rrbracket \times \llbracket 1, T \rrbracket$  as follows:

$$TRI_{i,j} = \frac{\sum_{k,l \in \mathcal{D}_3} |D_{i+k,j+l} - D_{i,j}|}{(3^2 - 1)}. \quad (4)$$

265 The Vector Ruggedness Measure (*VRM*) quantifies terrain ruggedness : slope and  
 266 aspect are decomposed into 3-dimensional vector components using standard vector  
 267 analysis in a user-specified moving  $3 \times 3$  window. The vector ruggedness measure is  
 268 dimensionless because it involves sine and cosine of the slope and aspect measures  
 269 and its values range from 0 to 1 corresponding to flat regions to rugged ones. Its  
 270 mathematical definition is omitted to avoid technicalities and details can be found in

271 (Sappington et al, 2007).  
 272 The Curvature position may also be linked to the nature of the seabed. It helps to  
 273 delimit regions of distinct habitat by identifying boundaries in the character of the  
 274 terrain ((Wilson et al, 2007)). Bathymetric Position Index (*BPI*), the marine version  
 275 of the topographic position index, quantifies where a location on a bathymetric surface  
 276 is relative to the overall seascape (Mata et al, 2021). It provides an indication of  
 277 whether any particular pixel forms part of a positive (e.g., crest) or negative (e.g.,  
 278 trough) feature of the surrounding terrain (Lundblad et al, 2006; Wilson et al, 2007).  
 279 It is calculated using the following formula, for each cell  $(i, j) \in \llbracket 1, T \rrbracket \times \llbracket 1, T \rrbracket$ :

$$BPI_{i,j} = D_{i,j} - \frac{\sum_{k,l \in \mathcal{D}_3} |D_{i+k,j+l} - D_{i,j}|}{(3^2 - 1)}. \quad (5)$$

280 According to (Evans, 1980), Profile convexity (*Prof<sub>c</sub>*) is the rate of change of *Slope*  
 281 and Plan convexity (*Plan<sub>c</sub>*) is the rate of change of *Aspect*. Negative values in the  
 282 *Prof<sub>c</sub>* indicate the surface is upwardly convex whereas, positive values indicate that  
 283 the surface is upwardly concave. Positive values in the *Plan<sub>c</sub>* means the surface is later-  
 284 ally convex and negative values indicate that the surface is laterally concave. Several  
 285 methods exist for numerical approximations of these metrics, based on a quadratic  
 286 form representation  $f$  of the surface (Florinsky, 1998; Horn, 1981; Evans, 1980; Zeven-  
 287 bergen and Thorne, 1987). Numerical implementation of (Zevenbergen and Thorne,  
 288 1987) method's is used in this study ; details can be found in (Florinsky, 1998).  
 289 All the computed terrain attributes, depth and geographic coordinates (longitude,  
 290 latitude) are then stacked to form a multilayer grid of predictors called features or  
 covariates in the sequel Table 1.

**Table 1** Terrain attributes computed from the DBM and functions used to do such calculations in R software

Terrain attributes	Reference	Function / R Package
<b>Slope and Aspect</b>		
Slope	(Horn, 1981)	terrain / raster
Aspect	(Horn, 1981)	terrain / raster
<b>Terrain Variability</b>		
Roughness	(Dartnell, 2000)	terrain / raster
Terrain Ruggedness Index ( <i>TRI</i> )	(Wilson et al, 2007)	terrain / raster
Vector Ruggedness Measure ( <i>VRM</i> )	(Ilich et al, 2023)	VRM / MultiscaleDTM
<b>Curvature and relative position</b>		
Profile Curvature ( <i>Prof<sub>c</sub></i> )	(Zevenbergen and Thorne, 1987)	Curvature / spatialEco
Planform Curvature ( <i>Plan<sub>c</sub></i> )	(Zevenbergen and Thorne, 1987)	Curvature / spatialEco
Bathymetric Position Index ( <i>BPI</i> )	(Ilich et al, 2023)	BPI / MultiscaleDTM

291

292 **2.2.3 Sampling**

293 To build predictive models for geomorphological typologies using a statistical learn-  
 294 ing approach, a training dataset is required. This one must contain a finite number of  
 295 ground truth locations and a set of predictive covariates for geomorphological typolo-  
 296 gies at these locations. In this section, three alternative clustering based sampling  
 297 methods are proposed to draw automatically these locations inside a given study area.  
 298 All these methods use cell’s centers of a regular grid and choose among the covariates  
 299 earlier mentioned depending on the choosen algorithm.

300 **Spatial Coverage Sampling using k-means clustering algorithm (SCS-  
 301 KMEANS)**

302 The basic idea of Spatial Coverage Sampling (SCS) is to draw uniformly sampling loca-  
 303 tions over the study area. It has been shown that SCS on a study area can be achieved  
 304 by k-means clustering algorithm (Hartigan, 1975). This consists in grouping cell’s cen-  
 305 ters of a regular grid on this area using their spatial coordinates as covariates. Note  
 306 that this regular grid can be the DBM one as long as it does not lead to computational  
 307 deadlock, otherwise it can be replaced by a raster grid with lower resolution. The final  
 308 solution of this partition gives the sampling locations and is determined by minimizing  
 309 a geometric criterion, the mean squared shortest distance between the clusters cen-  
 310 troids and the grid cell’s centers (Royle and Nychka, 1998; Brus et al, 2006). For the  
 311 implementation, a k-means algorithm for equal area partitioning is used (Brus, 2019).  
 312 The *scsKM* function provided in the supplemental materials can be used to achieve  
 313 this.

314 **Spatial Coverage Sampling using CLARA algorithm (SCS-CLARA)**

315 K-means clustering approach is time and storage consuming, especially for high DBM  
 316 resolution. In such case, CLARA algorithm approach could be an alternative. The  
 317 CLARA algorithm is an extension of the Partitioning Around Medoids (PAM) meth-  
 318 ods (Kaufman and Rousseeuw, 1975) to deal with data containing a large number of  
 319 objects (more than several thousand observations) in order to reduce computing time  
 320 and storage problem. Medoids  $(M_i)_{i=1}^k$  in a PAM,  $k$  being the desired number of clus-  
 321 ters  $C_i$ , are cells that minimize their distance to other cell’s centers of the cluster. The  
 322 CLARA algorithm generates  $j \in \mathbf{N}^*$  random samples of size  $n$  ( $n < T^2$ ) on individu-  
 323 als, applies a PAM on these samples one after the other, then evaluates the partition  
 324 quality on each of them by calculating the average global dissimilarity on the complete  
 325 dataset as follows:

$$\sum_{i=1}^k \sum_{x_c \in C_i} \frac{d(x_c, M_i)}{T^2} \quad (6)$$

326 If this dissimilarity is lower than the previous found one, it considers this solution and  
 327 its  $k$  medoids as the best current solution. The *scsCLARA* function in the supple-  
 328 mental materials can be used to choose ground truth locations.

329 **Complexity-Dependent Sampling using CLARA algorithm (CDS)**

330 Terrain morphology can sometime be marked by accidented region where many typolo-  
 331 gies are observed closed to each other. This is particularly true with coral reef region  
 332 where for example sand flat, reef slope, reef flat, etc typologies can be close to each

333 other. In such situations, homogeneous sampling would lead to miss many typolo-  
 334 gies unless a lot of points are requested leading to other problems such as important  
 335 unbalanced typologies distribution among locations (Brus, 2019). To account for such  
 336 typologies distribution, ground truth locations are agglomerated around zone of higher  
 337 ground complexity (i.e. complex terrain). Thus the CDS method is introduced in  
 338 order to take advantage of these covariates available for each DBM resolution. CDS  
 339 aims to distribute sampling locations around most heterogeneous or complex areas.  
 340 It uses DBM’s cells as individuals and unlike the SCS which uses the spatial coordi-  
 341 nates, CDS’s covariates are chosen among terrain attributes and depth. Depth and  
 342 Roughness measures are considered in this study. CDS cannot be computed using the  
 343 k-means clustering algorithm for high DBM resolutions because DBM cells are manda-  
 344 tory to get covariates. This is why the CLARA algorithm is only used. The *cdCLARA*  
 function in the supplemental materials can be used to this end (Figure 2).

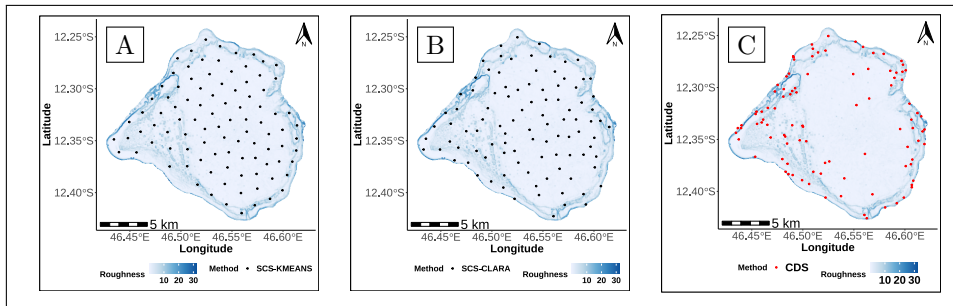


**Fig. 2** Example of 100 ground truth locations drawn with the different methods: **A** Spatial Coverage Sampling using K-means clustering algorithm (SCS-KMEANS), **B** Spatial Coverage Sampling using CLARA algorithm (SCS-CLARA) **C** and Complexity-dependant sampling using a CLARA algorithm (CDS). Roughness and Depth are used to guide the complexity-dependant sampling.

345

#### 346 2.2.4 Geomorphology mapping using Random Forest algorithm

347 To map geomorphological typologies over a whole study area, a supervised classifica-  
 348 tion approach is considered. This work was divided in two steps: a first step to train  
 349 algorithm and a second step to predict typologies based on trained algorithm. For  
 350 the training part, each location is generated by one of the previously described sam-  
 351 pling methods and typologies were attributed using the expert map Figure 1B. These  
 352 located typologies were the target variable, locations coordinates and the correspond-  
 353 ing depth and terrain attributes were used as covariates and both formed the training  
 354 dataset. In this process, a feature selection scheme random forest based is used to sub-  
 355 set the most relevant covariates of the training set. Then a final model is fitted using  
 356 the selected covariates. After this first step completed, the second step consisted in  
 357 using the fitted model to predict the most suitable typology over the whole study area.

##### 358 **The generic principle of Random Forest**

359 The tree based Random Forest (RF) algorithm can be used for a classification task

360 (Breiman, 2001; Biau and Scornet, 2016). Using the Bootstrap AGGREGatING (bag-  
361 ging) principle, RF increases the diversity of the trees by making them grow from  
362 different randomly drawn (with replacement) training datasets from the original  
363 dataset (Breiman, 1996). At each node of each tree, Rf selects a random subset of fea-  
364 tures and search for the best split for the node. To classify a new case once the forest  
365 is completed, the typology having the most votes over all the trees is retained.

#### 366 **Model training**

367 Using a cross-validation scheme with 3 repeats, the training samples are split into 3  
368 folds. To train a RF model, three hyperparameters were tuned: the number of trees  
369 (*Ntrees*) of the forest, the number of features used at each node (*Mtry*) and the min-  
370 imum number of data points at the terminal node of each tree (*nodesize*). Indeed,  
371 the *Ntrees* hyperparameter is not tunable in the classical sense but should be set suf-  
372 ficiently high (Díaz-Uriarte and Alvarez de Andrés, 2006; Oshiro et al, 2012; Probst  
373 et al, 2019). The default value of 500 trees is used. The *nodesize* hyperparameter has  
374 been set to 1 for classification task because it generally provides good results (Díaz-  
375 Uriarte and Alvarez de Andrés, 2006). The *Mtry* hyperparameter was tuned among  
376 fifteen values of hyperparameters chosen automatically by the function *tuneLength*.  
377 A random search optimization strategy which defines a search space as a bounded  
378 domain of parameter values and randomly sample points in that domain were used to  
379 find the optimal *Mtry* considering the the resulting Accuracy (Grandini et al, 2020).  
380 Models are fitted by repeatedly leaving out one of the folds and performance are deter-  
381 mined by predicting on the fold left out. The *train* function of the *caret* R package  
382 were used to this end.

#### 383 **Terrain attributes selection**

384 By selecting the most relevant terrain attributes as covariates, the risk of over fitting  
385 can be reduced and the model’s generalization ability improved. Variable or feature  
386 importance measures are usually used to rank or select variables. Mean Decrease Impu-  
387 rity (MDI) and Mean Decrease Accuracy (MDA) are two well-known random forest  
388 variable importance measures (Guyon and Elisseeff, 2020; Breiman, 2001; Biau and  
389 Scornet, 2016). In this study, the MDA measure also called permutation importance  
390 in Breiman’s original random forest is chosen since it seems to exhibit less bias than  
391 MDI in presence of correlated features (Strobl et al, 2008; Breiman, 2001). Roughly  
392 speaking, the MDA measure consists in shuffling values of a given covariate  $j$  in the  
393 test data or out-of-bag data (that is data excluded from the bootstrap sample used to  
394 construct the tree) and then computes the difference between the error on the per-  
395 muted test set and the original test set. More precisely, for each tree  $t$  among the  $ntree$   
396 trees of the RF, MDA uses the out-of-bag data to compute a prediction error  $OOB_t$ .  
397 Then, permuting the values of the  $j^{th}$  feature in the out-of-bag data, a prediction error  
398  $OOB_t^j$  is computed by using the permuted out-of-bag data. The permutation impor-  
399 tance of the feature  $j$  is thus defined by  $MDA_j = \frac{1}{ntree} \sum_{t=1}^{ntree} (OOB_t - OOB_t^j)$ .  
400 To achieve feature selection via the MDA measure, the backward Recursive Feature  
401 Elimination (RFE) algorithm (Guyon et al, 2002) implemented in the *rfe*<sup>4</sup> function  
402 of the *caret* R package is used. This algorithm is based on assessing MDA’s impor-  
403 tance. MDA is computed by iteratively permuting the values of each input covariate

---

<sup>4</sup><https://topepo.github.io/caret/recursive-feature-elimination.html>

404 and measuring the resulting drop in prediction accuracy. The feature with the mini-  
 405 mum MDA value, representing the least important feature, is systematically removed  
 406 from the input set. Subsequently, a new RF model is trained using this reduced set of  
 407 features. This process is continued until the minimal set of input features that yielded  
 408 optimal Accuracy (Grandini et al, 2020) is obtained. To improve the performance of  
 409 feature selection with RFE, a repeated 3-fold cross-validation with 3 repeats is used.  
 410 The *createFolds* function of the *caret* package allowed to split data into training and  
 411 test sets. This function carries a random sampling within geomorphological typologies  
 412 in order to balance the classes distributions within the split.  
 413 Once the model is trained, typologies can be predicted across the entire study area.  
 414 Typologies predictions are made using the *predict.train* function of the *caret* R  
 415 package (Kuhn, 2019).

### 416 2.2.5 Performance criteria

417 To assess model’s performance, a *Balanced Accuracy (BA)* metric were calculated  
 418 using the confusion matrix obtained from each model (Grandini et al, 2020). It consists  
 419 for each typology (class)  $k$ , to calculate a Recall score measuring the ability of a model  
 420 to find all the positive units for this class as follows:

$$Recall_k = \frac{TP_k}{TP_k + FN_k} \quad (7)$$

421 True Positives (TP) are observations predicted to belong to the reference class when  
 422 they really do, and False Negatives (FN) are observations predicted to not belong to  
 423 the reference class when they really do. *BA* gives an average measure of this concept  
 424 using the arithmetic mean of Recall across all classes :

$$BA = \frac{\sum_{k=1}^K Recall_k}{K} \quad (8)$$

425 where  $K$  is the total number of class  $k$ .

426 The number of unsampled typologies is used as an indicator of the efficiency of the  
 427 sampling method to visit all geomorphologic typologies present in the study area.

428 To assess the consistency of predictions, the map produced at the different DBM  
 429 resolution are compared to Expert map. For this purpose, the expert map is first  
 430 discretized into "pixels" size of 5 m resolution (ie. the smallest resolution used in  
 431 this study). Then the predicted map grid is disaggregated to match the expert map  
 432 resolution using *disagRast* function in the supplemental materials. To compare two  
 433 maps, two metrics are calculated using the confusion matrix between the two: *Match*  
 434 and *Balanced Match*.

435 The *Match* metric is a simple comparison between the two maps. The *Match* metric  
 436 corresponding to the proportion of cells identically labelled is calculated as follows:

$$Match = \frac{N_+}{N_+ + N_-} \quad (9)$$

437 Where  $N_+$  is the total number of cells where typologies match between the two maps,  
 438 and  $N_-$  is the total number of cells that do not match. The *matchRast* function is  
 439 proposed for the calculation of this metric. However such comparison might hide pre-  
 440 diction problems on some small surface typologies, totally dominated by high surface  
 441 coverage of some typologies. To take account of such fact, the *Balance Match* is a  
 442 sort of ponderated *Match* removing the surface dominant effect that some typologies  
 443 might have on others. A second metric denoted *Balanced Match (BM)* inspired by  
 444 the *BA* defined in Eq. 8 and using the confusion matrix between a predicted map and  
 445 the expert map is also calculated. Note that after disaggregating a predicted map,  
 446 some cells centers around the study site borders may be located outside. These border  
 447 effects are handled by proportioning *BA* to the proportion of cells  $L$  labelled after the  
 448 disaggregation of a predicted map. *BM* is calculated as follows:

$$BM = L \cdot \frac{\sum_{k=1}^K Recall_k}{K} \quad (10)$$

449 The *balmatchRast* function provided in the supplemental materials is used for the  
 450 *BM* calculation.

## 451 3 Results

### 452 3.1 Effect of ground truth sampling methodologies on 453 typologies sampled

454 Our first methodological assessment was to evaluate the number of missed typologies  
 455 on the expert map depending on ground truth sampling techniques. Unsurprisingly,  
 456 the more data points sampled, the greater the chance of sampling all typologies present  
 457 in the study site, regardless of the sampling method and the resolution of the DBM  
 458 (Figure 3). Whatever the sampling method and the DBM resolution, small sample  
 459 size (50 and 100 data points) do not allow to sample all typologies. For these sample  
 460 sizes, between 1 and 4 typologies are never sampled. It can also be noticed that for  
 461 500 data points sampled and more, all typologies are sampled no matter the sampling  
 462 method and the resolution of the DBM.

### 463 3.2 Assessment of model performance based on input data

464 The *Balanced Accuracy* criteria helps assessing model performance. The larger the  
 465 sample size, the more precise these measures (ie. smaller standard errors; Figure 4).  
 466 For small sample sizes (50 and 100 data points), sampling methods give comparable  
 467 results or even slightly better results for SCS-KMEANS than others sampling methods.  
 468 In constrast, from 200 points upwards, complexity-dependent sampling tends to give  
 469 better results than SCS-CLARA and SCS-KMEANS which give comparable results.  
 470 This result is confirmed as the sample size increases, with a widening gap among sam-  
 471 pling methodology means and decreasing standard errors (see Figure S3 and Table S3  
 472 for further details).



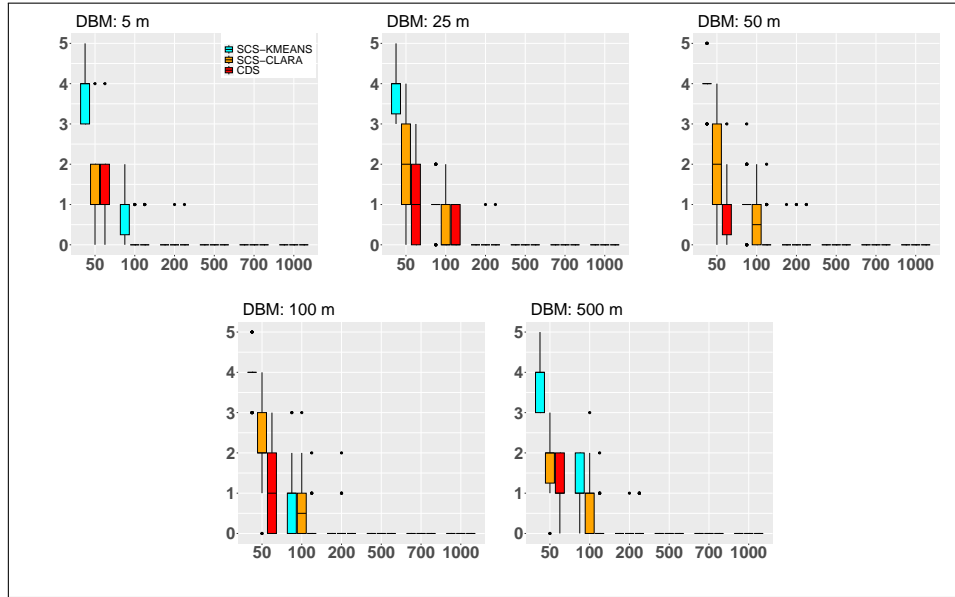


**Fig. 3** Boxplot representing the *Number of missing typologies* metric (y-axis) for different sample size (x-axis), different sampling methods (CDS, SCS-CLARA and SCS-KMEANS) and different bathymetric model resolutions (5 m, 25 m, 50 m, 100 m, 500 m). Each sampling conditions were replicated 30 times and represented as default R boxplot settings

### 473 3.3 Assessment of selected terrain attributes

474 A set of features is selected during the feature selection step of the modeling process  
 475 and general outputs are summarized. Only results for 100, 200, 500 data points sample  
 476 sizes generated at 100 m DBM resolution using SCS-CLARA method and CDS method  
 477 are shown here because they are representative of all results (Figure 5). Geographic  
 478 coordinates (*Latitude* and *Longitude*) and *Depth* are almost always selected regardless  
 479 the DBM resolution and the sampling method. Terrain variability attributes groups  
 480 (*Roughness*, *VRM* and *TRI*) that are selected a little more than half of the time.

### 481 3.4 Evaluation of the quality of produced maps

482 The *Match* criteria evaluates the consistency of predictions according to the expert  
 483 map. As previously seen with the *Balanced Accuracy* standard errors values, *Match*  
 484 errors are non negligible for small sample sizes and decrease when DBM resolutions  
 485 increase (Figure 6; Figure S3 and Table S4 for further details). In addition, lower  
 486 *Match* values are recorded at 5 m and 500 m DBM resolutions and higher *Match*  
 487 values were seen for intermediate DBM resolutions (25 m, 50 m, 100 m) regardless the  
 488 sample size.

489 When the sample size and the DBM resolution increase, *Balanced Match* val-  
 490 ues become more accurate as shown by a decrease of standard errors (Figure 7;  
 491 Figure S3 and Table S5 for further details). CDS method gives better results than

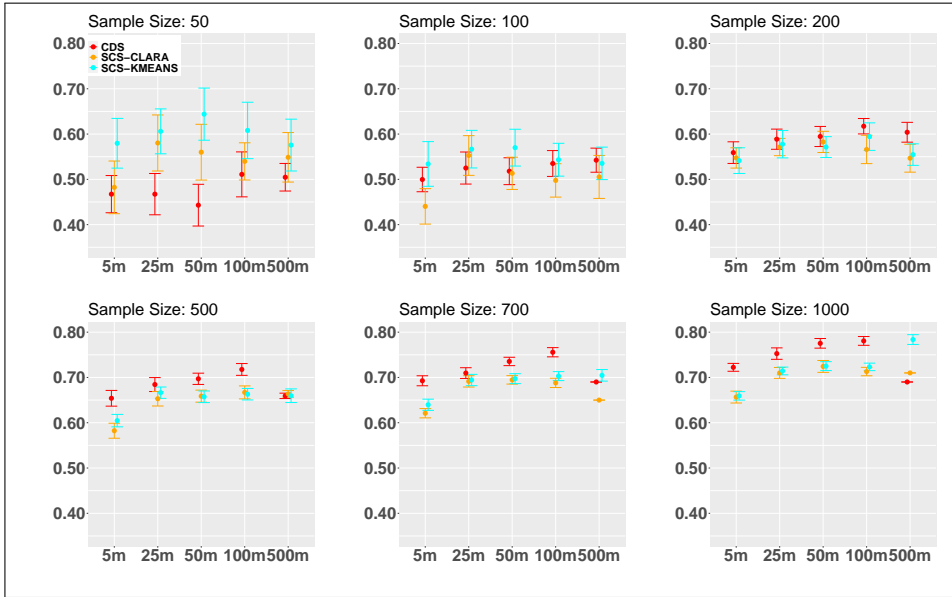


**Fig. 4** Mean (+/- standard error) over 30 draws of the *Balanced Accuracy* metric (y-axis) at different DBM resolutions (x-axis) for different sample size and different sampling methods (CDS, SCS-CLARA and SCS-KMEANS)

492 others spatial coverage sampling methods for any sample size and any DBM resolu-  
 493 tion. SCS-CLARA and SCS-KMEANS give comparable results according this criteria.  
 494 Comparing results among DBM resolutions, best results are achieved with 50 m and  
 495 100 m DBM resolutions.

496 In Figure 8 two maps generated with data points sampled using CDS methodology  
 497 are restituted: (A) 50 m DBM resolution using 1000 data points and (B) 100 m DBM  
 498 resolution using 200 data points. All typologies are sampled and predicted in both  
 499 cases. Results show that performance criteria measured are better for the (A') case  
 500 than the (B') case (see (C)). Indeed, some small surface typologies like Drowned sub-  
 501 tidal reef flat and inner slope are better predicted and predictions errors on typologies  
 502 transition areas less important for (A) than for (B).

## 503 4 Discussion

504 This methodology enabled us to successfully reconstruct an expert geomorphological  
 505 map. According to the *Number of missing typologies* metric, 200 data points are  
 506 enough to sample almost all the typologies. These locations can be chosen using  
 507 CDS which performs slightly better than spatial coverage sampling methods (SCS-  
 508 KMEANS and SCS-CLARA). Results between the different DBM resolutions are  
 509 comparable for small sample sizes considering the *Balanced Accuracy* metric. But, for  
 510 200 data points and more, 100 m DBM resolution gives clearly better results than oth-  
 511 ers resolutions. The *Match* metric supports this finding where 50 m and 100 m DBM

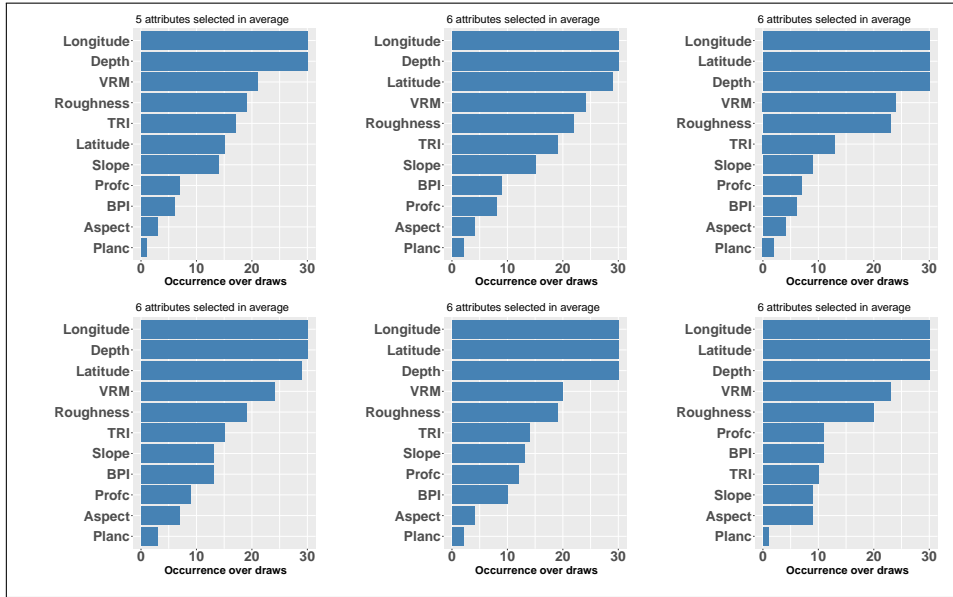


**Fig. 5** Ordered occurrence over 30 draws of the selected terrain attributes by the RFE algorithm. Here an example with 100, 200, 500 data points sample sizes (from left to right) generated at 100 m DBM resolution using SCS-CLARA method (top) and CDS method (bottom). The average number of attributes selected is noted above each graph (cf. Terrain attribute section for their definition)

512 resolutions gives much better results than others DBM resolutions whatever the number of data points. Considering the *Balanced Match* criteria which was introduced  
 513 to contrast the *Match* criteria taking into account typologies surface imbalances, 50  
 514 m DBM resolution gives a slight better performance than the 100 m DBM resolution,  
 515 but considering the sampling effort, it would be preferable to use the 100 m DBM.  
 516 Indeed, while the sampling effort is multiplied by 5 from (B) to (A), the performance  
 517 recorded is just a little bit better. We have also seen that the precision of the maps  
 518 produced is sensitive to the resolution of the DBM, the number and locations of the  
 519 ground truth selection. Thus, reproducible methodologies with associated codes to  
 520 evaluate their qualities are proposed. In this section, choices on data sampling to generate such maps are discussed. Then strong and weak points of the modeling approach  
 521 and alternative to enhance such work are addressed.  
 522  
 523

#### 524 4.1 Optimal data acquisition parameters

525 Creation of a submarine geomorphological map appears, among other consideration,  
 526 to be constrained between quantity and quality of initial data and cost to acquire  
 527 and process them. In the present work two kind of data fall in such compromise: the  
 528 bathymetric data and the ground truth data points.  
 529 For the bathymetric data acquisition, high resolution data require advanced tech-  
 530 nologies, longer survey durations, important storage and sophisticated tools for  
 531 manipulation which all contribute to higher costs. The results of this study show that  
 532 a lower DBM resolution do not necessarily lead to the best geomorphological map.

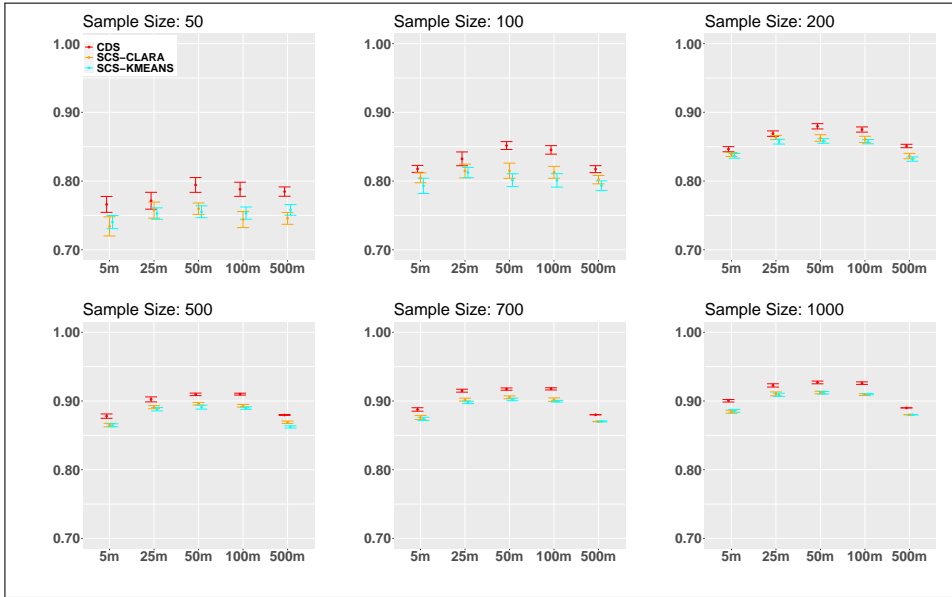


**Fig. 6** Mean (+/- standard error) over 30 draws of the *Match* metric (y-axis) at different DBM resolutions (x-axis) for different sample size and different sampling methods (CDS, SCS-CLARA and SCS-KMEANS)

533 The 100 m DBM resolution considered in this study appears to strike a good balance  
534 between detailed geomorphological maps obtained (Figures 4, 6, 7) with low DBM  
535 resolutions (5 and 25 m) and large scale geomorphological maps considering (500 m  
536 DBM resolution). Indeed, maps at 5 m, 25 m and 50 m DBM resolutions provide a  
537 reasonably detailed view of the seafloor and allow the identification of important fea-  
538 tures but contain a significant amount of noise or small-scale variability that may not  
539 be relevant in constructing a geomorphological map. On the other hand, maps of 500  
540 m resolution provide very generalized view of the seafloor representing a significantly  
541 coarser scale focusing on major landforms and regional-scale geomorphological pat-  
542 terns but missing important features required to build such maps (eg. reef patches,  
543 pass or canyons ...). The 100 m resolution was also considered suitable in previous  
544 studies for various applications, such as regional planning, environmental assessments,  
545 and natural hazard evaluations (Curie et al, 2007; Dong et al, 2019).  
546 Ground truth data acquisition is often acquired by specialists through scuba diving or  
547 snorkling (shallow) or using submarine, ROV or drop camera systems allowing to view  
548 and characterise seafloor typologies on specific location. In that respect, the number  
549 of location is directly correlated to cost of data gathering and therefore need to be  
550 balanced. Furthermore, if the number of data point is directly linked to survey cost,  
551 the location of sampling on an heterogeneous seafloor structure could be related to  
552 data quality (ie. enhanced typology sampling diversity above oversampling of common  
553 typologies). To test such compromises, effects number of data points and methodolo-  
554 gies to locate them (SCS vs CDS approach) on overall map quality production are

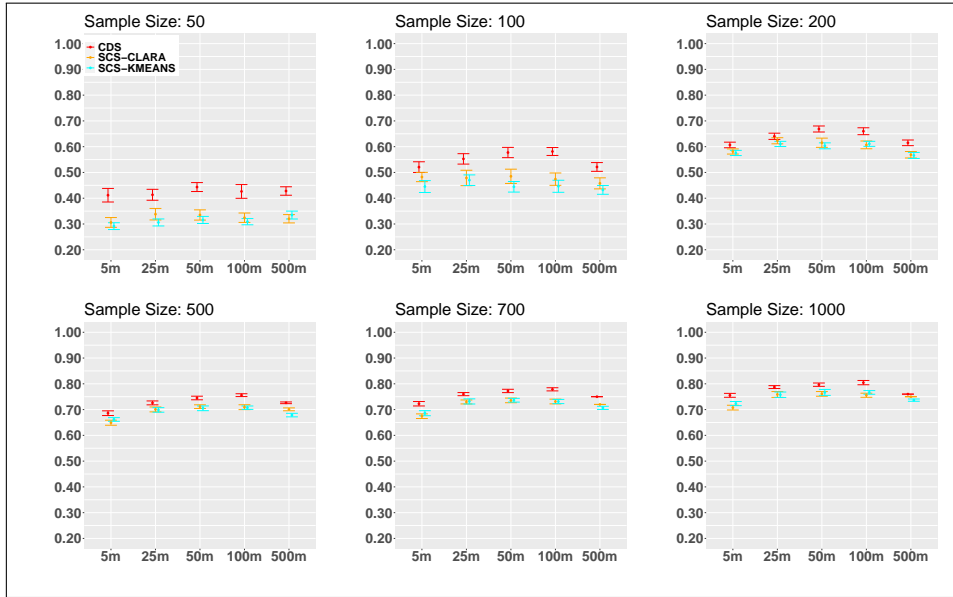


**Fig. 7** Mean (+/- standard error) over 30 draws of the *Balanced Match* metric (y-axis) at different DBM resolutions (x-axis) for different sample size and different sampling methods (CDS, SCS-CLARA and SCS-KMEANS).

555 studied. The choice between homogeneous distribution vs seafloor complexity depen-  
 556 dent approach came from the fact that various typologies might agglomerate around  
 557 location of complex structures (e.g. barrier reef, patch reef, ...). Figure 2 illustrates this  
 558 point and show that CDS method amplify sampling in area of important typologies  
 559 diversity. This explains why *Number of missing typologies* criteria results obtained  
 560 with CDS are better than homogeneous sampling methods (Figure 3). However, such  
 561 approach has the inconvenient that a bathymetric dataset is required prior planning  
 562 ground truth sampling campaign. Another point of attention is that attributes used  
 563 as covariates for CDS algorithms should be carefully selected. This study according to  
 564 the context of used data (coral reef habitats) focuses on metrics promoted in literature  
 565 (Adey, 1966; Adey and Macintyre, 1973; Battistini, 1975; Minnery et al, 1985) and  
 566 on empirical results from this work in the supplemental materials with a supervised  
 567 classification of geomorphologic typologies based on the terrain attributes presented  
 568 in Table 1. Seafloor depth and roughness were retained as the most relevant.  
 569 Evaluating effect of bathymetric data points density and number and location of  
 570 ground truth points was done by comparing produced map to an existing expert  
 571 manually made map. The *Match* criteria were introduced to see how realistic are pre-  
 572 dictions, regardless the number of sampled typologies. Thus the large geomorphologic  
 573 units like lagoons (deep, intermediate and shallow), subtidal and deep subtidal reef  
 574 flats are generally better predicted than the small surface typologies like Pass, Inner  
 575 slope, Outer slope and Drowned subtidal reef flat typologies. Indeed, such typologies  
 576 are under-represented in the study area and represent together no more than 10% of  
 577 the surface. Even evaluating the predictability of such typologies was difficult using

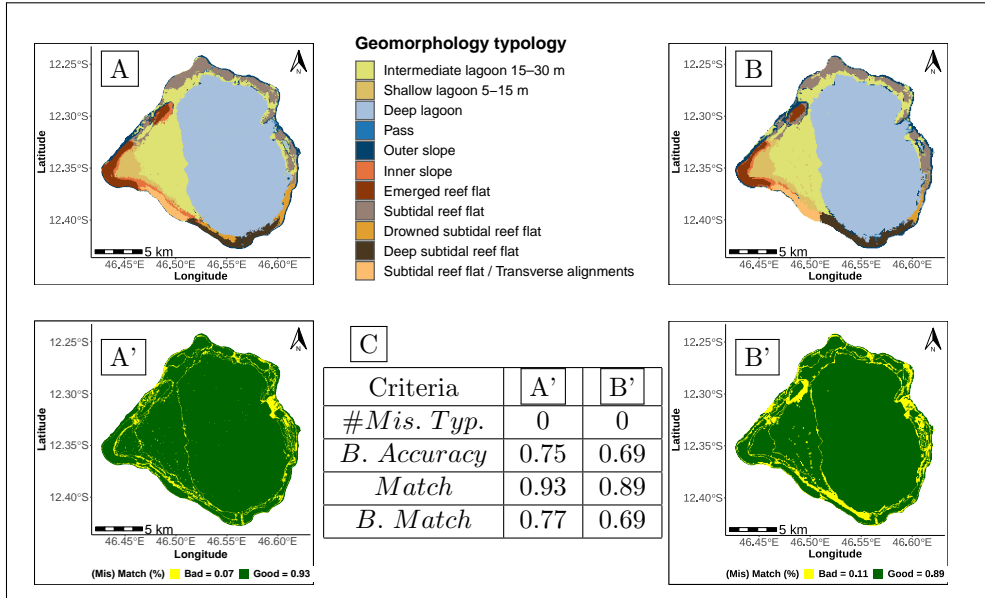


**Fig. 8** **A** Predicted map with a 50 m DBM and 1000 sampled locations using CDS methodology. **B** Predicted map with a 100 m DBM and 200 sampled locations using CDS methodology. Corresponding match / mismatch maps (A' and B') in comparison to the expert one. **C** Performance criteria measured.

578 the *Match* metric, hence the use of *Balanced Match* metric pondering typologies by  
579 their surface. Using both these metrics, optimal map construction was obtained for  
580 200 ground truth data points obtained using CDS methodology and 100 m DBM res-  
581 olution (Figure 8).

582 However, some limitation of the methodology used is to be noted. SCS-CLARA and  
583 CDS sampling methods are particularly useful for high dimensional data. The CLARA  
584 clustering algorithm can be used on large DBM grid cells data to generate ground truth  
585 locations. However, SCS-KMEANS although suitable for spatial coverage sampling,  
586 lead to computational deadlock for high DBM resolutions. Furthermore, it can not  
587 be used when there is missing data areas in the studied surface. Bathymetric imputa-  
588 tion of poorly sampled zones was done using ordinary kriging method that performed  
589 much better than others spatial interpolation methods (cf. Table S1, an example on  
590 the supplemental materials).

## 591 4.2 Modeling choices

592 Traditional approaches to build geomorphologic maps are often time-consuming, labor-  
593 intensive and has a limited coverage and scale. Remote Sensing techniques although  
594 allowing wide coverage and high-resolution, require expertise in image interpretation  
595 (Gao, 2009; Gilvear and Bryant, 2016). GIS approaches allow for the integration and  
596 analysis of diverse data types support data visualization and complex spatial anal-  
597 ysis. But they also require specialized software and expertise (Guzzetti et al, 1999;  
598 Napieralski and Li, 2007). In addition, interpretation and analysis heavily rely on data

599 quality. Besides these techniques, semi-automated and automated approaches through  
600 machine learning and deep learning are increasingly used to identify complex pat-  
601 terns and features for landform classification, feature detection, or segmentation. Deep  
602 learning models require large amounts of labeled training data (e.g., images, point  
603 clouds) to effectively learn complex patterns and relationships. Training such models  
604 involves adjusting millions of parameters through backpropagation and optimization  
605 algorithms (e.g., stochastic gradient descent) and their tuning involves finding the right  
606 network architecture and hyperparameters. They are often considered black boxes due  
607 to their complex architectures, making it challenging to interpret the features that  
608 influence predictions (Li et al, 2020). The statistical learning approach used in this  
609 study can handle large volumes of data, automate analysis processes and discover com-  
610 plex patterns and relationships in the data. Interpretability of used models may also  
611 be a challenge but less than deep learning ones. In addition, it can work effectively  
612 with smaller datasets which was crucial in our objectives.

613 RF model for geomorphologic units clustering is chosen because RF exhibits com-  
614 plex and non-linear relationships between the features and the dependent variable but  
615 also on features among themselves, handling effectively these relationships by using  
616 an ensemble of decision trees. It also provide valuable information as feature impor-  
617 tance measure helping identify the most informative feature which made it preferable  
618 to others clustering techniques in many cases. RF was used for supervised classifi-  
619 cation problems in many recent studies, compared different algorithms has shown  
620 effectiveness of RF based algorithms (Zeraatpisheh et al, 2017; Giaccone et al, 2022).  
621 It has shown its robustness specifically when data contain uncertainties and handles  
622 high-dimensional data efficiently avoiding overfitting and reducing computational com-  
623 plexity.

624 The variable selection step in the modeling procedure is crucial in the proposed  
625 methodology. Terrain attributes calculation is not specifically time-consuming but the  
626 relevance of each of them depends on the data and the geomorphological features that  
627 are mapped. This study demonstrated that the terrain attributes, although literature  
628 based choosen intially, have not all, a great explanatory power on geomorphologic fea-  
629 ture. For each generated sample, the number of features selected is also counted and  
630 6 terrain attributes are generally retained.

## 631 5 Conclusion

632 A statistical learning based approach is proposed to automatically map the geomor-  
633 phology of a study site using bathymetric data and some ground truth data points.  
634 On the one hand, tools to help geomorphologists to plan field campaigns in advance  
635 through an optimal DBM resolution and an automated sampling methodology to  
636 achieve field verifications are provided. On the other hand, a flexibility in the proposed  
637 methodology allowing the usage of terrain attributes as much as desired since the fea-  
638 ture selection will help to keep only the most relevant ones is preferred. In addition,  
639 statistical and computational tools to compare geomorphological maps produced at  
640 different resolutions are provided. The methodology reproducibility is made possible  
641 by a set of reusable R scripts.

642 In the future, an application of the methodology using others data available in oth-  
643 ers sites is planned. An investigation on others sampling methodology for e.g. which  
644 would take into account the presence of non sampling sites inside a study area is also  
645 being considered.

## 646 **6 Supplement information**

647 Additional figures and tables supporting this manuscript can be found after the  
648 Reference section.

## 649 **References**

650 Adey W (1966) Distribution of saxicolous crustose corallines in the northwestern north  
651 atlantic. *Journal of Phycology* 2:49–54. URL [https://doi.org/10.1111/j.1529-8817.](https://doi.org/10.1111/j.1529-8817.1966.tb04593.x)  
652 [1966.tb04593.x](https://doi.org/10.1111/j.1529-8817.1966.tb04593.x)

653 Adey W, Macintyre I (1973) Crustose coralline algae: A re-evaluation in the geological  
654 sciences. *Geological Society of America Bulletin* 84(3):883–904. URL [https://doi.](https://doi.org/10.1130/0016-7606(1973)84%3C883:CCAARI%3E2.0.CO;2)  
655 [org/10.1130/0016-7606\(1973\)84%3C883:CCAARI%3E2.0.CO;2](https://doi.org/10.1130/0016-7606(1973)84%3C883:CCAARI%3E2.0.CO;2)

656 Ahn S, Sung H, Han H (2023) Classification of the world undersea geomorphic features  
657 from gebco 2020 grid data. *Journal of the Korean Geographical Society* 58(1):36–54

658 Andréfouët S, Dirberg G (2006) Cartographie et inventaire du système récifal de  
659 wallis, futuna et alofi par imagerie satellitaire landsat 7 etm+ et orthophotogra-  
660 phies aériennes à haute résolution spatiale. IRD, Centre de Nouméa et Service de  
661 L’Environnement de Wallis et Futuna

662 Andréfouët S, Muller-Karger F, Robinson J, et al (2004) Global assessment of modern  
663 coral reef extent and diversity for regional science and management applications:  
664 a view from space. *Proceedings of the 10th International Coral Reef Symposium*  
665 2:1732–1745

666 Argyropoulou E, Argialas D, Nomikou P, et al (2016) Automatic identification of  
667 submarine landforms using object-based image analysis in the area of north aegan  
668 basin. *Bulletin of the Geological Society of Greece* 50(3):1605–1615. URL [https:](https://doi.org/10.12681/bgsg.11880)  
669 [//doi.org/10.12681/bgsg.11880](https://doi.org/10.12681/bgsg.11880)

670 Arhant Y, Neyt X, Pizurica A (2023) A new deep learning neural network architecture  
671 for seafloor characterisation. In *The 10th Military Sensing Symposium Proc*

672 Azarafza M, Azarafza M, Akgün PMH, and Atkinson, et al (2023) Deep learning-  
673 based landslide susceptibility mapping. *Scientific reports* 11(1):24112. URL [https:](https://doi.org/10.3390/su14031734)  
674 [//doi.org/10.3390/su14031734](https://doi.org/10.3390/su14031734)

675 Battistini R (1975) Eléments de terminologie récifale indopacifique. Station marine  
676 d’Endoume



- 677 Behrens T, Schmidt K, MacMillan R, et al (2018) Multi-scale digital soil mapping  
678 with deep learning. *Scientific reports* 8(1):15244. URL [https://doi.org/10.1038/  
679 s41598-018-33516-64](https://doi.org/10.1038/s41598-018-33516-64)
- 680 Biau G, Scornet E (2016) A random forest guided tour. *Test* 25:197–227. URL <https://doi.org/10.48550/arXiv.1511.05741>
- 682 Bishop M, James L, Shroder Jr J, et al (2012) Geospatial technologies and digital geo-  
683 morphological mapping: Concepts, issues and research. *Geomorphology* 137(1):5–26.  
684 URL <https://doi.org/10.1016/j.geomorph.2011.06.027>
- 685 Breiman L (1996) Bagging predictors. *Machine learning* 24:123–140. URL [https://doi.  
686 org/10.1007/BF00058655](https://doi.org/10.1007/BF00058655)
- 687 Breiman L (2001) Random forests. *Machine learning* 45:5–32. URL [https://doi.org/  
688 10.1023/A:1010933404324](https://doi.org/10.1023/A:1010933404324)
- 689 Breyer G, Bartholomä, A.Pesch R (2023) The suitability of machine-learning algo-  
690 rithms for the automatic acoustic seafloor classification of hard substrate habitats  
691 in the german bight. *Remote Sensing* 15(16):4113. URL [https://doi.org/10.3390/  
692 rs15164113](https://doi.org/10.3390/rs15164113)
- 693 Browne N, Smithers S, Perry C (2010) Geomorphology and community structure of  
694 middle reef, central great barrier reef, australia: an inner-shelf turbid zone reef  
695 subject to episodic mortality events. *Coral Reefs* 29:683–689. URL [https://doi.org/  
696 10.1007/s00338-010-0640-3](https://doi.org/10.1007/s00338-010-0640-3)
- 697 Brus D (2019) Sampling for digital soil mapping: A tutorial supported by r scripts.  
698 *Geoderma* 338:464–480. URL <https://doi.org/10.1016/j.geoderma.2018.07.036>
- 699 Brus D, De Gruijter J, Van Groenigen J (2006) Designing spatial coverage samples  
700 using the k-means clustering algorithm. *Developments in Soil Science* 31:183–192.  
701 [https://doi.org/https://doi.org/10.1016/S0166-2481\(06\)31014-8](https://doi.org/https://doi.org/10.1016/S0166-2481(06)31014-8)
- 702 Copeland A, Edinger E, Devillers R, et al (2013) Marine habitat mapping in support  
703 of marine protected area management in a subarctic fjord: Gilbert bay, labrador,  
704 canada. *Journal of Coastal Conservation* 17:225–237. URL [https://doi.org/10.1007/  
705 s11852-011-0172-1](https://doi.org/10.1007/s11852-011-0172-1)
- 706 Cressie N (1988) Spatial prediction and ordinary kriging. *Mathematical geology*  
707 20:405–421. URL <https://doi.org/10.1007/BF00892986>
- 708 Cui X, Liu H, Fan M, et al (2021) Seafloor habitat mapping using multibeam  
709 bathymetric and backscatter intensity multi-features svm classification frame-  
710 work. *Applied Acoustics* 174:107728. URL [http://dx.doi.org/10.1016/j.apacoust.  
711 2020.107728](http://dx.doi.org/10.1016/j.apacoust.2020.107728)

- 712 Curie F, Gaillard S, Ducharne A, et al (2007) Geomorphological methods to charac-  
713 terise wetlands at the scale of the seine watershed. *Science of the total environment*  
714 75(1-3):59–68. URL <https://doi.org/10.1016/j.scitotenv.2006.12.013>
- 715 Dartnell P (2000) Applying remote sensing techniques to map seafloor geology/habitat  
716 relationships. Masters Thesis, San Francisco State University
- 717 Dekavalla M, Argialas D (2017) Object-based classification of global undersea topog-  
718 raphy and geomorphological features from the srtm30 plus data. *Geomorphology*  
719 288:66–82. URL <http://dx.doi.org/10.1016/j.geomorph.2017.03.026>
- 720 Diesing M, Green S, Stephens D, et al (2014) Mapping seabed sediments: Compar-  
721 ison of manual, geostatistical, object-based image analysis and machine learning  
722 approaches. *Continental Shelf Research* 84:107–119. URL <https://doi.org/10.1016/j.csr.2014.05.004>
- 723
- 724 Dong Y, Liu Y, Hu C, et al (2019) Coral reef geomorphology of the spratly islands:  
725 A simple method based on time-series of landsat-8 multi-band inundation maps.  
726 *ISPRS Journal of Photogrammetry and Remote Sensing* 157:137–154. URL <https://doi.org/10.1016/j.isprsjprs.2019.09.011>
- 727
- 728 Dramis F, Guida D, Cestari A (2011) Nature and aims of geomorphological mapping.  
729 Developments in earth surface processes 15:39–73. URL <https://doi.org/10.1016/B978-0-444-53446-0.00003-3>
- 730
- 731 Díaz-Uriarte R, Alvarez de Andrés S (2006) Gene selection and classification of  
732 microarray data using random forest. *BMC bioinformatics* 7:1–13. URL <https://doi.org/10.1186/1471-2105-7-3>
- 733
- 734 Evans I (1980) An integrated system of terrain analysis and slope mapping. *Zeitschrift*  
735 *fur Geomorphologic Suppl-Bd* 36:274–295
- 736 Florinsky I (1998) Accuracy of local topographic variables derived from digital eleva-  
737 tion models. *International Journal of Geographical Information Science* 12(1):47–61.  
738 URL <https://doi.org/10.1080/136588198242003>
- 739 Fukunaga A, Craig B, Kosaki R (2019) Integrating three-dimensional benthic habi-  
740 tat characterization techniques into ecological monitoring of coral reefs. *Journal of*  
741 *Marine Science and Engineering* 7(2). URL <https://doi.org/10.3390/jmse7020027>
- 742 Galvez D, Papenmeier S, Sander L, et al (2022) Ensemble mapping as an alternative to  
743 baseline seafloor sediment mapping and monitoring. *Geo-Marine Letters* 42(3):11.  
744 URL <https://doi.org/10.1007/s00367-022-00734-x>
- 745 Gao J (2009) Bathymetric mapping by means of remote sensing: methods, accuracy  
746 and limitations. *Progress in Physical Geography* 33(1):103–116. URL <https://doi.org/10.1177/0309133309105657>
- 747

- 748 Giaccione E, Oriani F, Tonini M, et al (2022) Using data-driven algorithms for semi-  
749 automated geomorphological mapping. *Stochastic Environmental Research and Risk*  
750 *Assessment* 36:2115–2131. URL <https://doi.org/10.1007/s00477-021-02062-5>
- 751 Gilvear D, Bryant R (2016) Analysis of remotely sensed data for fluvial geomorphology  
752 and river science. *Tools in fluvial geomorphology* pp 103–132. URL [https://doi.org/](https://doi.org/10.1002/9781118648551.ch6)  
753 [10.1002/9781118648551.ch6](https://doi.org/10.1002/9781118648551.ch6)
- 754 Grandini M, Bagli E, Visani G (2020) Metrics for multi-class classification: an  
755 overview. arXiv preprint arXiv:200805756 URL [https://doi.org/10.48550/arXiv.](https://doi.org/10.48550/arXiv.2008.05756)  
756 [2008.05756](https://doi.org/10.48550/arXiv.2008.05756)
- 757 Guyon I, Elisseeff A (2020) An introduction to variable and feature selection.  
758 *Journal of machine learning research* 3:1157–1182. URL [https://doi.org/10.1162/](https://doi.org/10.1162/153244303322753616)  
759 [153244303322753616](https://doi.org/10.1162/153244303322753616)
- 760 Guyon I, Weston J, Barnhill S (2002) Gene selection for cancer classification using  
761 support vector machines. *Machine Learning* 46:389–422. URL [https://doi.org/10.](https://doi.org/10.1023/A:1012487302797)  
762 [1023/A:1012487302797](https://doi.org/10.1023/A:1012487302797)
- 763 Guzzetti F, Carrara A, Cardinali M, et al (1999) Landslide hazard evaluation: a review  
764 of current techniques and their application in a multi-scale study, central italy.  
765 *Geomorphology* 31(1-4):181–216. URL [https://doi.org/10.1016/S0169-555X\(99\)](https://doi.org/10.1016/S0169-555X(99)00078-1)  
766 [00078-1](https://doi.org/10.1016/S0169-555X(99)00078-1)
- 767 Hartigan J (1975) *Clustering algorithms*. John Wiley & Sons, Inc
- 768 Horn B (1981) Hill shading and the reflectance map. *Proceedings of the IEEE*  
769 69(1):14–47. URL <https://doi.org/10.1109/PROC.1981.11918>
- 770 Hugenholtz C, Whitehead K, Brown O, et al (2013) Geomorphological mapping with a  
771 small unmanned aircraft system (suas): Feature detection and accuracy assessment  
772 of a photogrammetrically-derived digital terrain model. *Geomorphology* 194:16–24.  
773 URL <https://doi.org/10.1016/j.geomorph.2013.03.023>
- 774 Ilich A, Misiuk B, Lecours V, et al (2023) Multiscaledtm: An open-source r package  
775 for multiscale geomorphometric analysis. *Transactions in GIS* 4:1164–1204. URL  
776 <https://doi.org/10.1111/tgis.13067>
- 777 Janowski L, Wroblewski R, Dworniczak J, et al (2021) Offshore benthic habitat map-  
778 ping based on object-based image analysis and geomorphometric approach. a case  
779 study from the slupsk bank, southern baltic sea. *Science of the Total Environment*  
780 801:149712. URL <https://doi.org/10.1016/j.scitotenv.2021.149712>
- 781 Janowski RL and Wroblewski, Rucinska M, Kubowicz-Grajewska A, et al (2022) Auto-  
782 matic classification and mapping of the seabed using airborne lidar bathymetry.  
783 *Engineering Geology* 301:106615. URL <https://doi.org/10.1016/j.enggeo.2022>

- 785 Jasiewicz J, Stepinski T (2013) Geomorphons—a pattern recognition approach to  
786 classification and mapping of landforms. *Geomorphology* 182:147–156. URL <https://doi.org/10.1016/j.geomorph.2012.11.005>  
787
- 788 Kaufman L, Rousseeuw P (1975) Partitioning around medoids (program pam).  
789 Finding groups in data: an introduction to cluster analysis 344:68–125
- 790 Kienholz H (1978) Maps of geomorphology and natural hazards of grindelwald,  
791 switzerland: Scale 1: 10,000. *Arctic and Alpine Research* 10(2):169–184
- 792 Koop L, Snellen M, Simons D (2021) An object-based image analysis approach using  
793 bathymetry and bathymetric derivatives to classify the seafloor. *Geosciences* 11:45.  
794 URL <https://doi.org/10.3390/geosciences11020045>
- 795 Kuhn M (2019) caret: Classification and regression training. URL <https://CRAN.R-project.org/package=caret>, r package, version 6.0-92. Accessed: 2023-03-28
- 797 Lacharité M, Brown C, Gazzola V (2018) Multisource multibeam backscatter data:  
798 developing a strategy for the production of benthic habitat maps using semi-  
799 automated seafloor classification methods. *Mar Geophys Res* 39:307–322. URL  
800 <https://doi.org/10.1007/s11001-017-9331-6>
- 801 Lecours V, Dolan M, Micallef A, et al (2016) A review of marine geomorphometry, the  
802 quantitative study of the seafloor. *Hydrology and Earth System Sciences* 20(8):3207–  
803 3244. URL <https://doi.org/10.5194/hess-20-3207-2016>
- 804 Leon J, Roelfsema C, Saunders M, et al (2015) Measuring coral reef terrain rough-  
805 ness using "structure-from-motion" close-range photogrammetry. *Geomorphology*  
806 242:21–28. URL <https://doi.org/10.1016/j.geomorph.2015.01.030>
- 807 Li S, Xiong L, Tang G, et al (2020) Deep learning-based approach for landform  
808 classification from integrated data sources of digital elevation model and imagery.  
809 *Geomorphology* 354:107045. URL <https://doi.org/10.1016/j.geomorph.2020.107045>
- 810 Locker S, Armstrong R, Battista T, et al (2010) Geomorphology of mesophotic coral  
811 ecosystems: current perspectives on morphology, distribution, and mapping strate-  
812 gies. *Coral Reefs* 29:329–345. URL <https://doi.org/10.1007/s00338-010-0613-6>
- 813 Lucieer V, Lucieer A (2009) Fuzzy clustering for seafloor classification. *Marine Geology*  
814 264(3-4):230–241. URL <https://doi.org/10.1016/j.margeo.2009.06.006>
- 815 Lundblad E, Wright D, Miller J, et al (2006) A benthic terrain classification scheme for  
816 american samoa. *Marine Geodesy* 29(2):89–111. <https://doi.org/https://doi.org/10.1080/01490410600738021>  
817

- 818 Maschmeyer C, White S, Dreyer B, et al (2019) High-silica lava morphology at ocean  
819 spreading ridges: Machine-learning seafloor classification at alarcon rise. *Geosciences*  
820 9(6):245. URL <https://doi.org/10.3390/geosciences9060245>
- 821 Masetti G, Mayer L, Ward L (2018) A bathymetry-and reflectivity-based approach  
822 for seafloor segmentation. *Geosciences* 8(1):14. URL [https://doi.org/10.3390/  
823 geosciences8010014](https://doi.org/10.3390/geosciences8010014)
- 824 Mata D, Úbeda J, Fernández-Sánchez A (2021) Modelling of the reef benthic habitat  
825 distribution within the cabrera national park (western mediterranean sea). *Annals*  
826 of GIS 27(3):285–298. URL <https://doi.org/10.1080/19475683.2021.1936169>
- 827 Van der Meij W, Meijles E, Marcos D, et al (2022) Comparing geomorphological  
828 maps made manually and by deep learning. *Earth Surface Processes and Landforms*  
829 47(4):1089–1107. URL <https://doi.org/10.1002/esp.5305>
- 830 Minnery G, Rezak R, Bright T (1985) Depth zonation and growth form of crustose  
831 coralline algae: flower garden banks, northwestern gulf of mexico. *Paleoalgology:*  
832 *Contemporary research and applications* Berlin, Heidelberg: Springer p 237–246.  
833 URL [https://doi.org/10.1007/978-3-642-70355-3\\_18](https://doi.org/10.1007/978-3-642-70355-3_18)
- 834 Minár J, Evans I (2008) Elementary forms for land surface segmentation: The the-  
835 oretical basis of terrain analysis and geomorphological mapping. *Geomorphology*  
836 95(3-4):236–259. URL <https://doi.org/10.1016/j.geomorph.2007.06.003>
- 837 Misiuk B, Brown C (2023) Improved environmental mapping and validation using bag-  
838 ging models with spatially clustered data. *Ecological Informatics* 77:102181. URL  
839 <https://doi.org/10.1016/j.ecoinf.2023.102181>
- 840 Misiuk B, Diesing M, Aitken A, et al (2021) A spatially explicit comparison  
841 of quantitative and categorical modelling approaches for mapping seabed sedi-  
842 ments using random forest. *Annals of GIS* 9(6):254. URL [https://doi.org/10.3390/  
843 geosciences9060254](https://doi.org/10.3390/geosciences9060254)
- 844 Napieralski JJ. Harbor, Li Y (2007) Glacial geomorphology and geographic informa-  
845 tion systems. *Earth-Science Reviews* 85(1-2):1–22. URL [https://doi.org/10.1016/j.  
846 earscrev.2007.06.003](https://doi.org/10.1016/j.earscrev.2007.06.003)
- 847 Novaczek E, Devillers R, Edinger E (2019) Generating higher resolution regional  
848 seafloor maps from crowd-sourced bathymetry. *Plos one* 14(6):e0216792. URL <https://doi.org/10.1371/journal.pone.0216792>
- 850 Oshiro T, Perez P, Baranauskas J (2012) How many trees in a random forest? *Machine*  
851 *Learning and Data Mining in Pattern Recognition MLDM 2012 Lecture Notes in*  
852 *Computer Science()*, Springer, Berlin, Heidelberg 7376. URL [https://doi.org/10.  
853 1007/978-3-642-31537-4\\_13](https://doi.org/10.1007/978-3-642-31537-4_13)

- 854 Otto JC, Smith M (2013) Geomorphological mapping, vol Section 2.6, British Society  
855 for Geomorphology, chap 2, pp 1–10
- 856 Otto JC, Prasicek G, Blöthe J, et al (2018) Gis applications in geomorphology. In:  
857 Comprehensive geographic information systems. Elsevier, p 81–111, URL [10.1016/  
858 B978-0-12-409548-9.10029-6](https://doi.org/10.1016/B978-0-12-409548-9.10029-6)
- 859 Pandian P, Ruscoe J, Shields M, et al (2009) Seabed habitat mapping techniques:  
860 an overview of the performance of various systems. *Mediterranean Marine Science*  
861 10(2):29–44. URL <https://doi.org/10.12681/mms.107>
- 862 Pavlopoulos K, Evelpidou N, Vassilopoulos A (2009) Mapping geomorphological  
863 environments. Springer Science & Business Media URL [https://doi.org/10.1007/  
864 978-3-642-01950-0](https://doi.org/10.1007/978-3-642-01950-0)
- 865 Probst P, Wright M, Boulesteix A (2019) Hyperparameters and tuning strategies  
866 for random forest. *Wiley Interdisciplinary Reviews: data mining and knowledge  
867 discovery* 9(3):e1301. URL <https://doi.org/10.1002/widm.1301>
- 868 Riley S, DeGloria S, Elliot R (1999) Index that quantifies topographic heterogeneity.  
869 *intermountain Journal of sciences* 5(1-4):23–27
- 870 Roberts D (2015) Spatially balanced subsampling in r (retaining max-  
871 imum sample size). [https://davidrroberts.wordpress.com/2015/09/25/  
872 spatial-buffering-of-points-in-r-while-retaining-maximum-sample-size/](https://davidrroberts.wordpress.com/2015/09/25/spatial-buffering-of-points-in-r-while-retaining-maximum-sample-size/)
- 873 Roos D, Dupont P, Gaboriau M, et al (2017) Projet epicure : Etude des peuplements  
874 ichtyologiques et des communautés récifales à partir d’indicateurs spatiaux et de  
875 l’approche fonctionnelle, des bancs du geyser, de la zélée et de l’iris. URL <https://doi.org/10.13155/54549>  
876
- 877 Royle J, Nychka D (1998) An algorithm for the construction of spatial coverage designs  
878 with implementation in splus. *Computers & Geosciences* 24(5):479–488
- 879 Rozycka M, Migon P, Michniewicz A (2017) Topographic wetness index and terrain  
880 ruggedness index in geomorphic characterisation of landslide terrains, on examples  
881 from the sudetes, sw poland. *Zeitschrift für geomorphologie, supplementary issues*  
882 61(2):61–80
- 883 Sappington J, Longshore K, Thompson D (2007) Quantifying landscape ruggedness  
884 for animal habitat analysis: A case study using bighorn sheep in the mojave desert.  
885 *Journal of Wildlife Management* 71(5):1419–1426. URL [https://doi.org/10.2193/  
886 2005-723](https://doi.org/10.2193/2005-723)
- 887 Schmidt J, Hewitt A (2004) Fuzzy land element classification from dtms based on  
888 geometry and terrain position. *Geoderma* 121(3-4):243–256. URL [https://doi.org/  
889 10.1016/j.geoderma.2003.10.008](https://doi.org/10.1016/j.geoderma.2003.10.008)

- 890 Siart C, Bubenzer O, Eitel B (2009) Combining digital elevation data (srtm/aster),  
891 high resolution satellite imagery (quickbird) and gis for geomorphological map-  
892 ping: A multi-component case study on mediterranean karst in central crete.  
893 *Geomorphology* 112(1-2):106–121. URL [https://doi.org/10.1016/j.geomorph.2009.](https://doi.org/10.1016/j.geomorph.2009.05.010)  
894 [05.010](https://doi.org/10.1016/j.geomorph.2009.05.010)
- 895 Siqueira R, Veloso G, Fernandes-Filho E, et al (2022) Evaluation of machine learning  
896 algorithms to classify and map landforms in antarctica. *Earth Surface Processes*  
897 *and Landforms* 47(2):367–382. URL <https://doi.org/10.1002/esp.5253>
- 898 Sklar E, Bushuev E, Misiuk B, et al (2024) Seafloor morphology and substrate mapping  
899 in the gulf of st lawrence, canada, using machine learning approaches. *Frontiers in*  
900 *Marine Science* 11:1306396. URL <https://doi.org/10.3389/fmars.2024.1306396>
- 901 Sowers D, Masetti G, Mayer L, et al (2020) Standardized geomorphic classification of  
902 seafloor within the united states atlantic canyons and continental margin. *Frontiers*  
903 *in Marine Science* 7:9. URL <https://doi.org/10.3389/fmars.2020.00009>
- 904 Stepinski T, Ghosh S, Vilalta R (2007) Machine learning for automatic mapping  
905 of planetary surfaces. *Aquatic Conservation: Marine and Freshwater Ecosystems*  
906 30(4):846–859. URL <http://dx.doi.org/10.13140/2.1.1518.9445>
- 907 Sterne T, Retchless D, Allee R, et al (2020) Predictive modelling of mesophotic habi-  
908 tats in the north-western gulf of mexico. *Proceedings of the National Conference on*  
909 *Artificial Intelligence* 22(2):1807. URL <https://doi.org/10.1002/aqc.3281>
- 910 Strobl C, Boulesteix A, Kneib T, et al (2008) Conditional variable importance for  
911 random forests. *BMC bioinformatics* 9:1–11. URL <https://doi.org/10.1002/aqc.3281>
- 912 Summers G, Lim A, Wheeler A (2021) A scalable, supervised classification of seabed  
913 sediment waves using an object-based image analysis approach. *Remote Sensing*  
914 13(12):2317. URL <https://doi.org/10.3390/rs13122317>
- 915 Valentine P, Fuller S, Scully L (2004) Terrain ruggedness analysis and distribution of  
916 boulder ridges in the stellwagen bank national marine sanctuary region (poster).  
917 Galway, Ireland: 5th International Symposium on Marine Geological and Biological  
918 Habitat Mapping (GeoHAB)
- 919 Wabnitz C, Andréfouët S, Torres-Pulliza D, et al (2008) Regional-scale seagrass habi-  
920 tat mapping in the wider caribbean region using landsat sensors: Applications to  
921 conservation and ecology. *Remote Sensing of Environment* 112(8):3455–3467. URL  
922 <https://doi.org/10.1016/j.rse.2008.01.020>
- 923 Wilson M, O’CONNELL B, Brown C, et al (2007) Multiscale terrain analysis of  
924 multibeam bathymetry data for habitat mapping on the continental slope. *Marine*  
925 *Geodesy* 30:3–35. <https://doi.org/10.1080/01490410701295962>, URL [https://doi.](https://doi.org/10.1080/01490410701295962)  
926 [org/10.1080/01490410701295962](https://doi.org/10.1080/01490410701295962)

- 927 Wynn R, Huvenne V, Le Bas T, et al (2014) Autonomous underwater vehicles (auvs):  
928 Their past, present and future contributions to the advancement of marine geo-  
929 science. *Marine geology* 352:451–468. URL [https://doi.org/10.1016/j.margeo.2014.](https://doi.org/10.1016/j.margeo.2014.03.012)  
930 [03.012](https://doi.org/10.1016/j.margeo.2014.03.012)
- 931 Zeraatpisheh M, Ayoubi S, Jafari A, et al (2017) Comparing the efficiency of dig-  
932 ital and conventional soil mapping to predict soil types in a semi-arid region in  
933 iran. *Geomorphology* 285:186–204. URL [https://doi.org/10.1016/j.geomorph.2017.](https://doi.org/10.1016/j.geomorph.2017.02.015)  
934 [02.015](https://doi.org/10.1016/j.geomorph.2017.02.015)
- 935 Zevenbergen L, Thorne C (1987) Quantitative analysis of land surface topography.  
936 *Earth Surface Processes and Landforms* 12:47–56. URL [https://doi.org/10.1002/](https://doi.org/10.1002/esp.3290120107)  
937 [esp.3290120107](https://doi.org/10.1002/esp.3290120107)



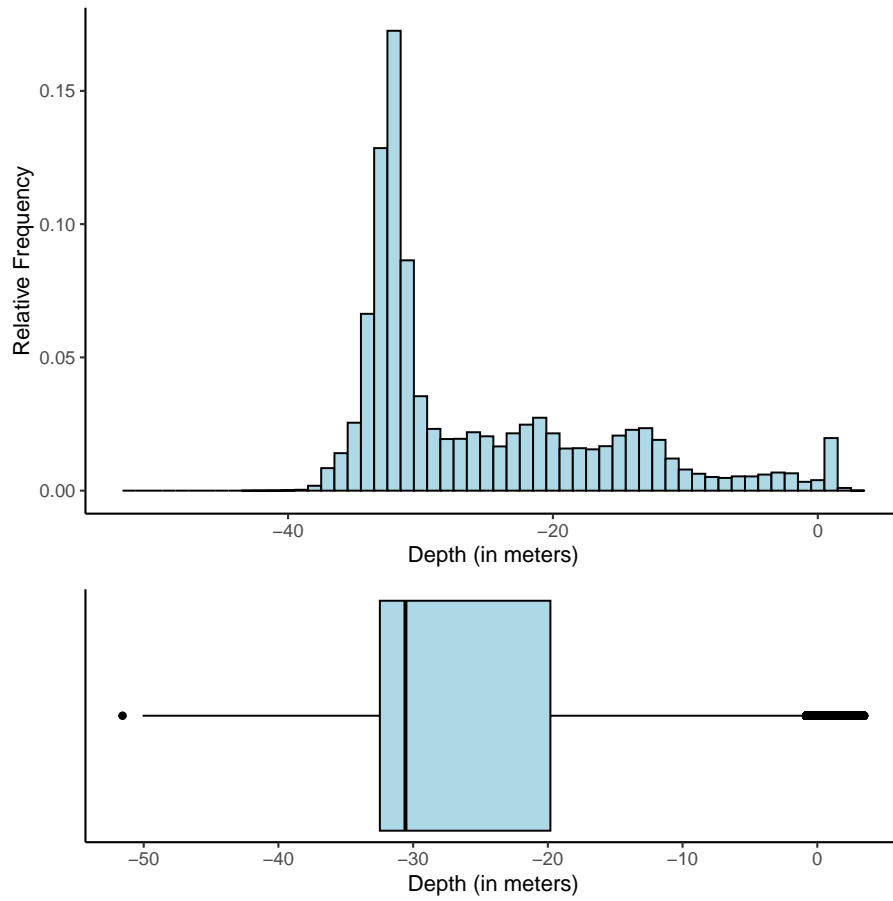


**Fig. S1** Distribution of the raw bathymetric data collected on Geyser.

**Table S1** Bathymetry imputation of empty grid cells of a 50 m DBM resolution. The Root Mean Squared Error (RMSE) and its Standard Deviation (SD) were calculated using 5-folds cross-validation scheme for five (05) spatial interpolation models : Inverse Distance Weighted (IDW), Nearest Neighbor (NN), Ordinary Kriging (OK), Universal Kriging (UK), Spatial GAM (GAM)

Method	RMSE	SD (RMSE)
IDW	0.80	0.02
NN	0.82	0.02
<b>OK</b>	<b>0.69</b>	<b>0.01</b>
UK	0.71	0.01
GAM	1.34	0.01

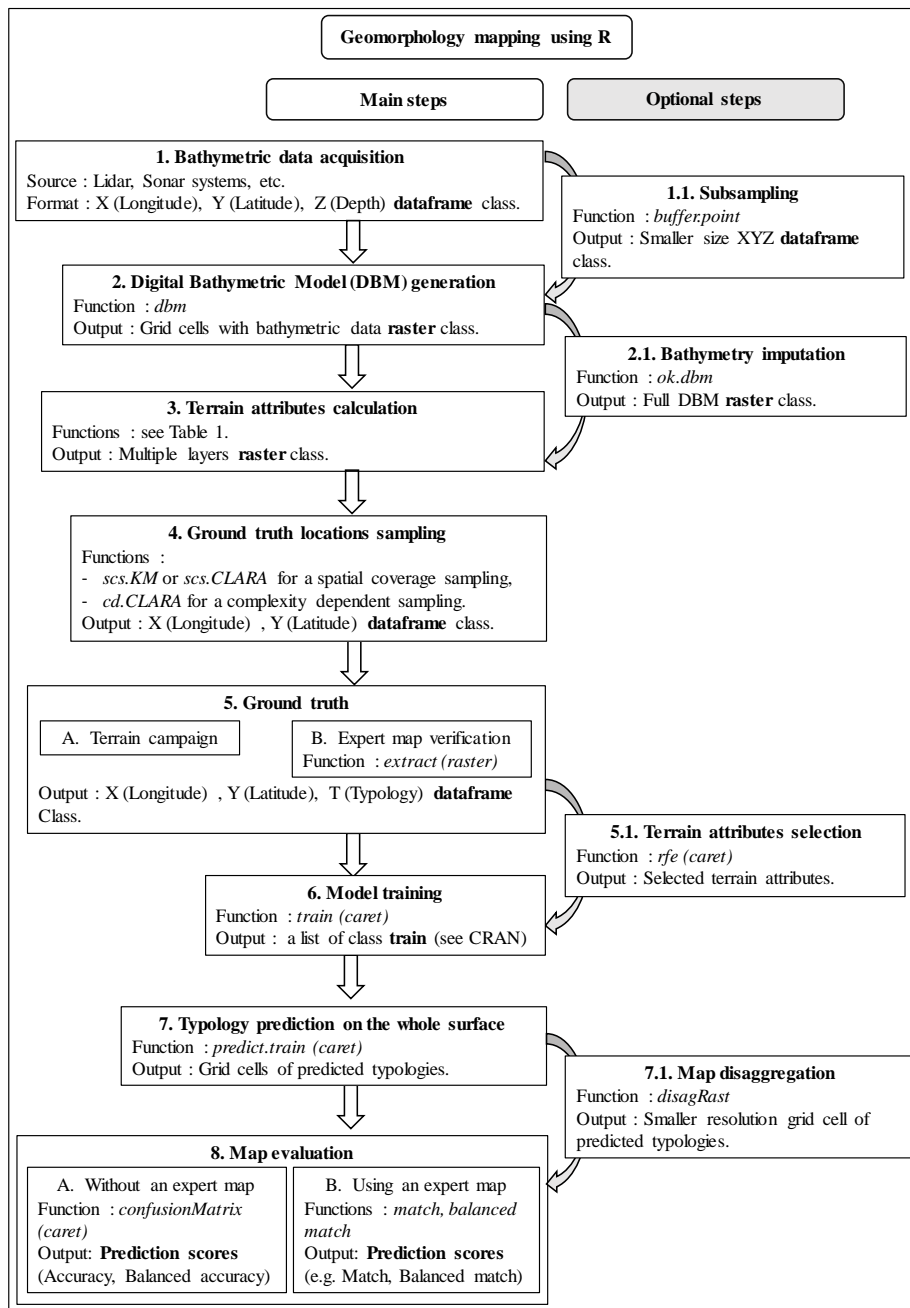


**Fig. S2** Statistical learning approach to build geomorphological maps using bathymetric data and typology field verification samples.

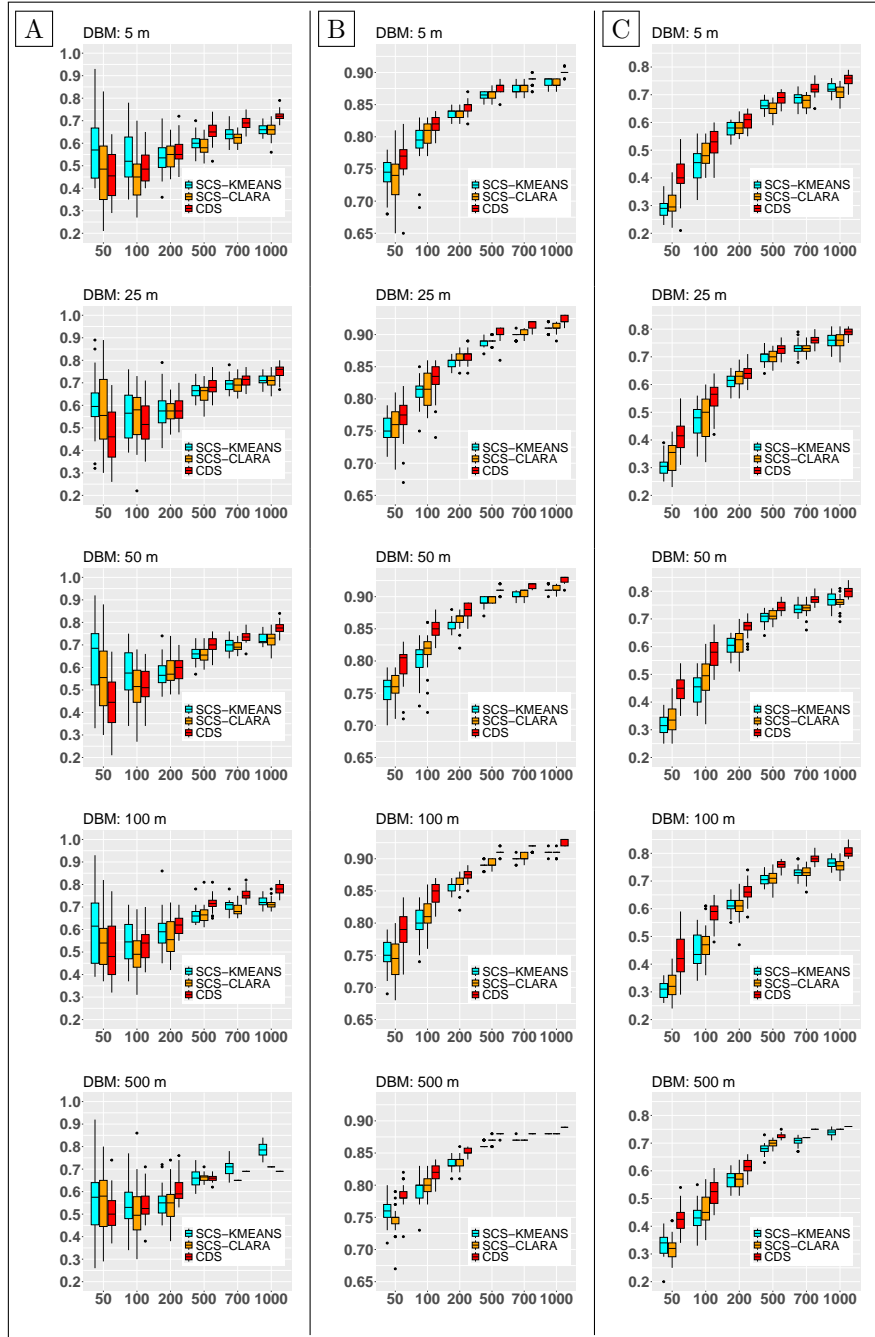


**Fig. S3** Boxplot of *Balanced Accuracy* (A), *Match* (B) and *Balanced Match* (C) metrics (y-axis) for different sample size (x-axis), different sampling methods (CDS, SCS-CLARA and SCS-KMEANS) and different bathymetric model resolutions (5 m, 25 m, 50 m, 100 m, 500 m). Each sampling conditions were replicated 30 times and represented as default R boxplot settings.

**Table S2** Mean (standard deviation) over 30 draws of the *Number of missing typologies* metric (y-axis) at different DBM resolutions (x-axis) for different sample size and different sampling methods (CDS, SCS-CLARA and SCS-KMEANS)

<b>DBM: 5 m</b>						
Method	Sample Size					
	50	100	200	500	700	1000
SCS-KMEANS	3.867 (0.681)	0.967 (0.718)	0 (0)	0 (0)	0 (0)	0 (0)
SCS-CLARA	5.033 (0.964)	2.133 (0.937)	0.633 (0.615)	0 (0)	0 (0)	0 (0)
CDS	3.067 (0.944)	0.967 (0.964)	0.167 (0.379)	0 (0)	0 (0)	0 (0)

<b>DBM: 25 m</b>						
Method	Sample Size					
	50	100	200	500	700	1000
SCS-KMEANS	6 (0.643)	3.1 (0.885)	0.533 (0.629)	0 (0)	0 (0)	0 (0)
SCS-CLARA	5.233 (0.898)	2.367 (0.964)	0.567 (0.626)	0 (0)	0 (0)	0 (0)
CDS	3.3 (1.179)	1.467 (0.9)	0.3 (0.466)	0 (0)	0 (0)	0 (0)

<b>DBM: 50 m</b>						
Method	Sample Size					
	50	100	200	500	700	1000
SCS-KMEANS	5.933 (0.74)	3.167 (0.791)	0.6 (0.724)	0 (0)	0 (0)	0 (0)
SCS-CLARA	5.067 (0.868)	2.1 (1.125)	0.567 (0.679)	0 (0)	0 (0)	0 (0)
CDS	2.833 (1.053)	0.933 (0.828)	0.233 (0.43)	0 (0)	0 (0)	0 (0)

<b>DBM: 100 m</b>						
Method	Sample Size					
	50	100	200	500	700	1000
SCS-KMEANS	5.867 (0.681)	3.033 (0.85)	0.567 (0.728)	0 (0)	0 (0)	0 (0)
SCS-CLARA	5 (0.947)	2.2 (0.805)	0.7 (0.702)	0.033 (0.183)	0 (0)	0 (0)
CDS	2.867 (1.252)	0.2 (0.407)	0.133 (0.346)	0 (0)	0 (0)	0 (0)

<b>DBM: 500 m</b>						
Method	Sample Size					
	50	100	200	500	700	1000
SCS-KMEANS	5.467 (0.73)	2.733 (0.785)	0.467 (0.507)	0 (0)	0 (0)	0 (0)
SCS-CLARA	4.8 (1.031)	2.367 (1.129)	0.4 (0.563)	0 (0)	0 (0)	0 (0)
CDS	3.133 (1.042)	1.433 (0.817)	0.233 (0.43)	0 (0)	0 (0)	0 (0)

**Table S3** Mean (standard deviation) over 30 draws of the *Balanced Accuracy* metric (y-axis) at different DBM resolutions (x-axis) for different sample size and different sampling methods (CDS, SCS-CLARA and SCS-KMEANS)

<b>DBM: 5 m</b>						
Method	Sample Size					
	50	100	200	500	700	1000
SCS-KMEANS	0.58 (0.147)	0.534 (0.132)	0.541 (0.076)	0.605 (0.037)	0.64 (0.033)	0.659 (0.025)
SCS-CLARA	0.482 (0.156)	0.44 (0.105)	0.547 (0.06)	0.582 (0.044)	0.621 (0.027)	0.657 (0.035)
CDS	0.467 (0.11)	0.5 (0.072)	0.559 (0.064)	0.654 (0.047)	0.693 (0.03)	0.722 (0.023)

<b>DBM: 25 m</b>						
Method	Sample Size					
	50	100	200	500	700	1000
SCS-KMEANS	0.606 (0.133)	0.567 (0.111)	0.578 (0.081)	0.666 (0.034)	0.694 (0.033)	0.714 (0.023)
SCS-CLARA	0.58 (0.166)	0.553 (0.118)	0.571 (0.051)	0.653 (0.043)	0.691 (0.034)	0.71 (0.032)
CDS	0.467 (0.122)	0.525 (0.095)	0.589 (0.06)	0.684 (0.041)	0.71 (0.032)	0.753 (0.034)

<b>DBM: 50 m</b>						
Method	Sample Size					
	50	100	200	500	700	1000
SCS-KMEANS	0.644 (0.154)	0.57 (0.109)	0.571 (0.062)	0.657 (0.034)	0.697 (0.029)	0.725 (0.026)
SCS-CLARA	0.56 (0.165)	0.513 (0.095)	0.583 (0.063)	0.659 (0.036)	0.695 (0.025)	0.724 (0.035)
CDS	0.443 (0.123)	0.518 (0.079)	0.595 (0.059)	0.697 (0.033)	0.735 (0.025)	0.775 (0.028)

<b>DBM: 100 m</b>						
Method	Sample Size					
	50	100	200	500	700	1000
SCS-KMEANS	0.608 (0.167)	0.543 (0.097)	0.594 (0.081)	0.663 (0.034)	0.703 (0.027)	0.723 (0.022)
SCS-CLARA	0.54 (0.11)	0.498 (0.099)	0.566 (0.084)	0.667 (0.038)	0.688 (0.027)	0.713 (0.025)
CDS	0.511 (0.133)	0.535 (0.076)	0.617 (0.046)	0.718 (0.035)	0.756 (0.027)	0.781 (0.026)

<b>DBM: 500 m</b>						
Method	Sample Size					
	50	100	200	500	700	1000
SCS-KMEANS	0.576 (0.153)	0.535 (0.096)	0.555 (0.064)	0.66 (0.04)	0.705 (0.034)	0.784 (0.029)
SCS-CLARA	0.549 (0.146)	0.505 (0.127)	0.547 (0.082)	0.664 (0.02)	0.65 (0)	0.71 (0)
CDS	0.505 (0.082)	0.542 (0.071)	0.604 (0.059)	0.659 (0.016)	0.69 (0)	0.69 (0)

**Table S4** Mean (standard deviation) over 30 draws of the *Match* metric (y-axis) at different DBM resolutions (x-axis) for different sample size and different sampling methods (CDS, SCS-CLARA and SCS-KMEANS)

<b>DBM: 5 m</b>						
Method	Sample Size					
	50	100	200	500	700	1000
SCS-KMEANS	0.74 (0.026)	0.793 (0.03)	0.837 (0.009)	0.865 (0.006)	0.874 (0.006)	0.886 (0.006)
SCS-CLARA	0.734 (0.037)	0.805 (0.019)	0.839 (0.008)	0.865 (0.007)	0.876 (0.008)	0.884 (0.006)
CDS	0.766 (0.031)	0.818 (0.014)	0.846 (0.01)	0.878 (0.008)	0.888 (0.007)	0.9 (0.005)

<b>DBM: 25 m</b>						
Method	Sample Size					
	50	100	200	500	700	1000
SCS-KMEANS	0.753 (0.022)	0.812 (0.02)	0.857 (0.009)	0.888 (0.007)	0.898 (0.005)	0.909 (0.006)
SCS-CLARA	0.758 (0.031)	0.815 (0.027)	0.863 (0.008)	0.891 (0.006)	0.902 (0.006)	0.91 (0.008)
CDS	0.771 (0.033)	0.832 (0.027)	0.869 (0.011)	0.902 (0.01)	0.915 (0.006)	0.923 (0.006)

<b>DBM: 50 m</b>						
Method	Sample Size					
	50	100	200	500	700	1000
SCS-KMEANS	0.755 (0.023)	0.801 (0.025)	0.858 (0.009)	0.891 (0.008)	0.902 (0.005)	0.912 (0.005)
SCS-CLARA	0.76 (0.023)	0.815 (0.03)	0.863 (0.013)	0.896 (0.005)	0.905 (0.006)	0.912 (0.005)
CDS	0.794 (0.029)	0.852 (0.015)	0.88 (0.01)	0.91 (0.005)	0.917 (0.004)	0.927 (0.005)

<b>DBM: 100 m</b>						
Method	Sample Size					
	50	100	200	500	700	1000
SCS-KMEANS	0.753 (0.024)	0.801 (0.026)	0.857 (0.008)	0.89 (0.005)	0.9 (0.003)	0.91 (0.003)
SCS-CLARA	0.744 (0.031)	0.813 (0.023)	0.861 (0.012)	0.893 (0.005)	0.902 (0.007)	0.909 (0.004)
CDS	0.788 (0.028)	0.845 (0.017)	0.875 (0.01)	0.91 (0.004)	0.918 (0.004)	0.926 (0.005)

<b>DBM: 500 m</b>						
Method	Sample Size					
	50	100	200	500	700	1000
SCS-KMEANS	0.758 (0.021)	0.793 (0.019)	0.832 (0.008)	0.862 (0.004)	0.87 (0.002)	0.88 (0)
SCS-CLARA	0.746 (0.023)	0.802 (0.016)	0.836 (0.01)	0.869 (0.005)	0.87 (0)	0.88 (0)
CDS	0.785 (0.018)	0.817 (0.014)	0.851 (0.007)	0.88 (0.002)	0.88 (0)	0.89 (0)

**Table S5** Mean (standard deviation) over 30 draws of the *Balanced Match* metric (y-axis) at different DBM resolutions (x-axis) for different sample size and different sampling methods (CDS, SCS-CLARA and SCS-KMEANS)

<b>DBM: 5 m</b>						
Method	Sample Size					
	50	100	200	500	700	1000
SCS-KMEANS	0.292 (0.035)	0.445 (0.062)	0.576 (0.027)	0.662 (0.019)	0.686 (0.026)	0.723 (0.021)
SCS-CLARA	0.306 (0.051)	0.482 (0.048)	0.581 (0.027)	0.649 (0.026)	0.674 (0.024)	0.708 (0.025)
CDS	0.412 (0.071)	0.521 (0.056)	0.607 (0.029)	0.686 (0.024)	0.723 (0.023)	0.755 (0.02)

<b>DBM: 25 m</b>						
Method	Sample Size					
	50	100	200	500	700	1000
SCS-KMEANS	0.306 (0.036)	0.47 (0.055)	0.611 (0.027)	0.699 (0.024)	0.732 (0.027)	0.758 (0.028)
SCS-CLARA	0.338 (0.06)	0.479 (0.08)	0.623 (0.032)	0.701 (0.025)	0.73 (0.021)	0.759 (0.03)
CDS	0.413 (0.057)	0.553 (0.054)	0.64 (0.032)	0.726 (0.02)	0.76 (0.016)	0.787 (0.015)

<b>DBM: 50 m</b>						
Method	Sample Size					
	50	100	200	500	700	1000
SCS-KMEANS	0.316 (0.037)	0.444 (0.055)	0.603 (0.031)	0.705 (0.025)	0.736 (0.02)	0.767 (0.031)
SCS-CLARA	0.335 (0.053)	0.485 (0.074)	0.615 (0.048)	0.711 (0.019)	0.736 (0.024)	0.761 (0.024)
CDS	0.443 (0.046)	0.577 (0.053)	0.669 (0.031)	0.745 (0.019)	0.772 (0.017)	0.797 (0.017)

<b>DBM: 100 m</b>						
Method	Sample Size					
	50	100	200	500	700	1000
SCS-KMEANS	0.309 (0.032)	0.446 (0.063)	0.611 (0.026)	0.707 (0.018)	0.731 (0.022)	0.767 (0.019)
SCS-CLARA	0.324 (0.049)	0.474 (0.064)	0.607 (0.04)	0.709 (0.025)	0.731 (0.025)	0.756 (0.021)
CDS	0.426 (0.071)	0.581 (0.041)	0.66 (0.036)	0.756 (0.015)	0.779 (0.016)	0.805 (0.022)

<b>DBM: 500 m</b>						
Method	Sample Size					
	50	100	200	500	700	1000
SCS-KMEANS	0.335 (0.041)	0.432 (0.046)	0.566 (0.031)	0.679 (0.018)	0.707 (0.016)	0.737 (0.012)
SCS-CLARA	0.32 (0.043)	0.458 (0.057)	0.569 (0.034)	0.701 (0.015)	0.72 (0)	0.75 (0)
CDS	0.428 (0.044)	0.521 (0.046)	0.615 (0.029)	0.726 (0.009)	0.75 (0)	0.76 (0)